Anomalous transport and upscaling in critically-connected fracture networks under stress conditions

Chuanyin Jiang, Delphine Roubinet, Qinghua Lei, Yanyong Wang, Xiaoguang Wang

Anomalous transport and upscaling in critically-connected fracture networks under stress conditions

Chuanyin Jiang[a], Delphine Roubinet[b,*], Qinghua Lei[c], Yanyong Wang[d,e], Xiaoguang Wang[d,e]

[a] *HydroSciences Montpellier, University of Montpellier, CNRS, IRD, Montpellier, France*
[b] *Geosciences Montpellier, University of Montpellier, CNRS, Montpellier, France*
[c] *Geohydrology Group, Department of Earth Sciences, Uppsala University, Uppsala, Sweden*
[d] *State Key Laboratory of Oil and Gas Reservoir Geology and Exploitation, Chengdu University of Technology, Chengdu, China*
[e] *Tianfu Yongxing Laboratory, Chengdu, China*

Abstract

Anomalous transport in fractured rocks is of high importance for numerous research fields and applications in hydrogeology and has been widely studied in the last decades. This phenomenon is due to the structural heterogeneities of fractured rocks and the high contrast between the fractures and matrix properties. At the same time, the fracture properties in terms of fracture density and geometrical characteristics are related to in-situ stress conditions that impact the connectivity of the system and the distributions of fracture aperture and length, including the creation of new cracks when the differential stress conditions are strong enough. In order to understand how all these features impact the observed anomalous transport, we study the role of in-situ stress in mass transport through a two-dimensional fractured rock. The fracture network is based on a real outcrop with a connectivity state around the percolation threshold, over which we simulate stress-dependent fracture deformation and propagation, and perform hydrodynamic transport through the deformed rock mass. The impact of the changes in aperture and the creation of new cracks on transport behavior is evaluated for various stress scenarios and reproduced with upscaled representations of transport processes. We also consider matrix diffusion as a source of anomalous transport and demonstrate that this process can be incorporated into the proposed upscaled

models. Resutls showed that traditional upscaling methods with space-Lagrangian velocities description capture well the Gaussian-like breakthrough curves (BTCs) under low-stress ratio conditions, but fail under high-stress ratio conditions with multiple-peak early-times BTCs. To characterize the emergence of strong anomalous transport, we extend the Random Walk model Directed by a Markov Process with space-Lagrangian velocity sampling by incorporating multiple transition matrices conditioned by different initial velocity states. This new transport upscaling model shows high accuracy in predicting complex transport behaviors in critically connected fracture networks.
Keywords: anomalous transport, natural fracture network, in-situ stress, fracture network topology, particle tracking, upscaling

Highlights

- High-stress conditions lead to multiple-peak early-times anomalous transport behavior
- Traditional upscaling methods fail to reproduce this anomalous transport behavior
- A new upscaling method succeeds in reproducing fracture networks anomalous transport
- This method reproduces high-stress and matrix diffusion anomalous transport behavior

1. Introduction

Flow and solute transport in heterogeneous fracture systems have become an important research subject in the past decades as the accurate characterization and prediction of flow and transport behaviors are involved in various engineering applications, such as groundwater remediation, geological storage of carbon dioxide, geothermal development,

*Corresponding author: delphine.roubinet@umontpellier.fr

and nuclear waste disposal [e.g., Tran et al., 2021, Yoo et al., 2021, Wang et al., 2023, Liu et al., 2022]. However, due to the fact that fractures exist at all scales, it seems impossible to accurately capture the transport behaviors based on the fine description of discrete fracture network (DFN) modeling for all scenarios of fracture systems, especially at a large scale. The potential uncertainty in the characterization of fractured media greatly challenges the practical value of DFN modeling [e.g., Demirel et al., 2019, Dorn et al., 2012, Zhou et al., 2021, Gattinoni and Scesi, 2018]. Therefore, developing upscaling methods, that are able to parameterize the transport model with a few characteristic parameters and be used for multi-scale prediction, has attracted increasing interest.

For the non-reactive solute (i.e., tracers) at the Darcy scale, the advection-dispersion equation (ADE) is the traditional approach to characterize the flow and transport behaviors when the breakthrough curves (BTC) exhibit a diffusion-like (Fickian) process [Bear, 2013]. However, the traditional approach is not always valid due to the emergence of anomalous (non-Fickian) transport with the BTCs characterized by early arrivals and long tails. The anomalous transport behaviors have been observed at various scales, from pore to single fracture and rock core column, and finally to field scale [e.g., Cortis and Berkowitz, 2004, Kang et al., 2015b, 2016, Gouze et al., 2020, 2023]. Therefore, some alternative models have been developed to address this issue [e.g., Berkowitz, 2002, Neuman, 2005, Noetinger et al., 2016]. Methods relying on the displacement of particles are particularly well suited for this matter. It includes random walk (RW) simulations that sample from fitted velocity distributions to reproduce the particle spreading pattern in two-dimensional DFNs, continuous time-random walk (CTRW) formalism that provides semi-analytical results for plume evolution, and Markov-directed random walk (MDRW) method that considers the necessity of sequential correlation along the trajectory [Berkowitz and Scher, 1997, 1998, Painter and Cvetkovic, 2005, Smith and Schwartz, 1984]. More recently, a spatial Markov model has also been used to develop a correlated CTRW model, which successfully characterizes the impact

of velocity distribution and correlation on transport in theoretical and field-scale fractured media [Kang et al., 2011, 2015a,b]. In addition, some alternative models are developed to fit BTCs by modifying the traditional advection-dispersion equation such as Mobile-Immobile (MI) model, Multiple Rate (MR) model and Multiple Region Advection-Dispersion (MRAD) model, which have shown a good ability to reproduce breakthrough curves obtained from the laboratory experiments [Majdalani et al., 2015, Wang et al., 2020] or numerical simulations [Davit et al., 2010, Cherblanc et al., 2007] via a proper parameter tuning. In addition to these alternative transport models, the importance of heterogeneities and uncertainties in stochastic quantification and modeling has been underlined in several studies [Riva et al., 2008, Schiavo, 2023].

Although the existing transport models successfully predict anomalous transport through DFNs, the rock heterogeneity in most of those works is generated randomly, both in terms of the geometric topology of the fracture network and the aperture distribution [Kang et al., 2015a, 2017, Painter and Cvetkovic, 2005]. In reality, subsurface fractures are inevitably subject to in-situ ground stress which is the essential factor in determining fracture aperture. Previous studies regarding the mechanical simulations of fractured rocks have indicated that the presence of fracture networks may lead to a non-uniform distribution of local stresses, which in turn produces various geomechanical responses to fractures, such as varying degrees of normal closure, shear sliding, dilatancy and crack propagation [Baghbanan and Jing, 2008, Lei and Gao, 2018, Liu et al., 2018, Min et al., 2004]. Consequently, hydraulic properties (i.e., flow distribution and bulk permeability) of the stress-controlled fractured rocks are affected, where the shear dilation under an anisotropic stress condition may lead to highly localized flows and increase the bulk permeability [Lei et al., 2017a, Min et al., 2004]. Recently, our study further shows that crack propagation induced by shearing may expand the flow backbone network and reduce the flow localization, and then significantly enhance the bulk permeability [Jiang et al., 2019]. In other studies, the impact of in-situ stress on anomalous

transport is investigated for single in-situ stress scenarios through studies that either focus on the importance of fracture growth [Nick et al., 2011] or consider dense fracture networks at the representative elementary volume scale [Rutqvist et al., 2013, Zhao et al., 2013]. Systematic analysis of various in-situ stress regimes is conducted in 2D and 3D fracture networks [Kang et al., 2019, Sweeney and Hyman, 2020, Zhao et al., 2011], whose transport properties are upscaled with a new dual-correlation-length CTRW approach in Kang et al. [2019] without considering the impact of matrix diffusion. The latter studies are based on the assumption of no stress-driven crack growth that holds in well-connected fracture networks, for which in-situ stress loading mainly causes the deformation of pre-existing fractures. However, this assumption is questionable when working with fracture networks whose connectivity is close to the percolation threshold, which is often observed in realistic domains [Lei and Wang, 2016, Renshaw, 1997].

In order to fully explore the impact of in-situ stress on anomalous transport in realistic fracture networks, we apply various stress conditions on critically-connected fracture networks that are based on a real outcrop. The role of stress-driven crack growth is considered and the effects of the stress orientation and magnitude on anomalous transport behavior are analyzed. The results presented in this work show the need for a new upscaling method that is provided to represent the observed anomalous transport behavior compared to existing models. The impact of matrix diffusion on anomalous transport in the considered stress scenarios is also illustrated and added to the proposed upscaling method.

This paper is organized as follows. The methodology of this work, including the considered fracture network, the geomechanical, fluid flow and transport models, and the upscaling method, is described in Section 2. The results of the numerical simulations in terms of anomalous transport with and without the effect of stress-driven new cracks are presented with the comparison of different upscaling models in Section 3. Finally, discussion and conclusions are provided in Section 4.

2. Methodology

2.1. Fracture network and geomechanical models

We consider the well-known outcrop collected at the Hornelen Basin in Norway [Odling, 1997] that corresponds to a critically connected network [Bour and Davy, 1997, Lei and Gao, 2018] characterized by three major fracture sets of orientation 5°, 50°, and 120° (Figure 1). The geometric connectivity of a fracture network can be characterized by a statistical parameter, i.e, the percolation parameter, $p = \frac{1}{L^2}\sum l^2$, where L is the modeling domain length and l is the length of individual fractures. A higher p means a more connected fracture network and the network is statistically connected once p exceeds the percolation threshold p_c, which may have a scale-independent value around 5.8 [Bour and Davy, 1997]. Here, the studied fracture network has a p of 5.6, which is critically connected. The fractured rock is a Devonian age sandstone consisting of more than 2000 joints, which are mostly perpendicular to the bedding plane. The readers can refer to numerous existing studies to gather information about the geometrical distribution of the fractures [Berkowitz et al., 2000, Bour, 2002] and the system behaviors in terms of stress variability [Lei and Gao, 2019], fluid flow [Jiang et al., 2019, Odling, 2001], and thermal transport [Geiger and Emmanuel, 2010].

For the geomechanical modeling, we use the same methodology as in geomechanical work previously conducted on this 2D fracture network [Lei and Gao, 2019, Jiang et al., 2019] where the relevant equations and settings of material properties, as well as the implementation, can be found in detail. Here, we consider the stress loading directions θ = 50°, 80°, 120°, and 150° (Figure 1a), which are denoted *Config1*, *Config2*, *Config3*, and *Config4*, respectively. The stress loading directions are aligned with one of the major fracture sets for *Config1* and *Config3*, and in between the main fracture set orientations for *Config2* and *Config4*. We also consider various stress conditions that have been defined in Jiang et al. [2019]. These conditions are reported in Table 1 and applied to each configuration.

	Iso1	*Iso2*	*Anis1*	*Anis2*	*Anis3*
$S_{\min}$	0	5	5	5	5
$S_{\max}$	0	5	10	15	20

Table 1: Isotropic (*Iso1* and *Iso2*) and anisotropic (*Anis1*, *Anis2*, and *Anis3*) stress scenarios considered with $S_{\max}$ the strength applied in the loading direction and $S_{\min}$ in the orthogonal direction, both expressed in MPa.

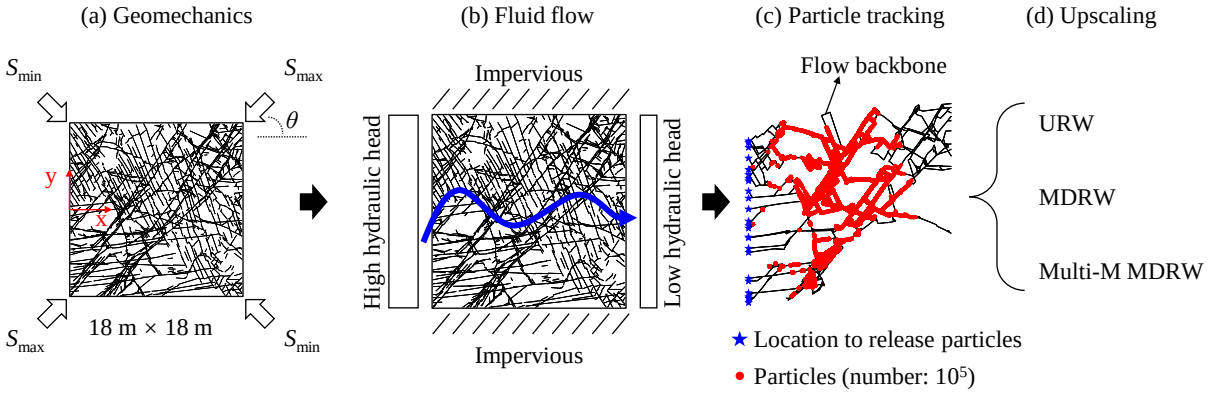

Figure 1: Modeling steps and boundary conditions for the (a) geomechanical, (b) fluid flow, (c) particle tracking, and (d) upscaling models, the latter being named Upscaled Random Walk (URW), Markov-Directed Random Walk (MDRW) and Multiple Matrices MDRW (Multi-M MDRW).

2.2. Hydrodynamic transport models

As done in numerous existing studies [e.g., Demirel et al., 2019, de Dreuzy et al., 2001, Roubinet et al., 2020], the fluid flow simulation is conducted by solving laminar and incompressible Darcy-type flow in fractured media with the fracture permeability governed by the cubic law [Witherspoon et al., 1980]. Here, we assume that the rock matrix is impervious to fluid flow, such that flow and advective transport only occur within the fractures while diffusion is considered in the rock matrix [Zhao et al., 2011]. A constant macroscopic hydraulic gradient is imposed by setting the hydraulic head on the left ($x = 0$ m) and right ($x = L$, L being the domain size set to 18 m) boundaries to 0 m and 18 m, respectively, and by prescribing no-flow conditions to the top and bottom boundaries (Figure 1b). Both fluid flow and particle tracking simulations are based on the flow backbone fractures where the dead ends are removed (Figure 1c). The fracture flow rate between nodes i and j is defined as $Q_{ij} = \delta\rho g a_{ij}^3 (h_j - h_i)/(12\mu l_{ij})$ where δ is the thickness of the fractured rock (assumed to

be 1 m for convenience), a_{ij} the local aperture, h_k the hydraulic head at node k ($k = i, j$), l_{ij} the length between nodes i and j, ρ the fluid density, μ the fluid dynamic viscosity, and g the gravitational acceleration. The hydraulic head at each node is computed by imposing mass conservation and the flow velocity between nodes i and j is computed as $u_{ij} = Q_{ij}/\left(a_{ij} \times \delta\right)$.

Solute transport in the fracture network is modeled by injecting 10^5 particles on the left border of the domain, that migrate through the fracture network by advection until reaching the right border of the domain (Figure 1c). The effect of matrix diffusion is considered by introducing a retention time t_{diff} added to the advection time based on the assumption of infinite matrix [Painter and Cvetkovic, 2005, Roubinet et al., 2010]:

$$t_{\text{diff}} = \left(\frac{\phi_{\text{m}}\sqrt{D_{\text{m}}}}{2\alpha b} t_a\right)^2, \tag{1}$$

where ϕ_{m} is the matrix porosity, D_{m} the molecular diffusion coefficient, b the half aperture of the fracture, and $\alpha = \text{erfc}^{-1}(U[0,1])$ with $U[0,1]$ being a uniform random number drawn between 0 and 1. At fracture intersections, we apply a complete mixing rule where the probability for a particle exiting an outgoing link is proportional to the flow rate through that link. The solute spreading behavior across the entire domain is quantified by the breakthrough curve recorded at the outlet of the domain and defined as the probability density function (PDF) of particle arrival time τ_b on the right side of the domain. The results presented in this work are obtained by considering $\phi_{\text{m}} = 0.05$ and $D_{\text{m}} = 10^{-8}$ m^2/s, and we verified that the same results are obtained for 10^5 and 10^6 particles, ensuring that the number of particles is high enough to correctly sample the considered domains.

2.3. Upscaled transport models

We consider existing upscaled transport models that are based on a set of spatial and temporal jumps, which are recorded during the fracture-network scale simulations. The 1D upscaled simulations are run by sampling into this database of spatial jumps until the sum of

these jumps exceeds the domain size L, and the predicted breakthrough time is expressed as the sum of the corresponding time steps. Among the existing upscaled transport models, we consider the Upscaled Random Walk (URW) and Markov-Directed Random Walk (MDRW) methods that are based on space-Lagrangian velocity statistics [Kang et al., 2017, 2019] and sequential velocity correlation [Painter and Cvetkovic, 2005], respectively. We also consider that the URW method can rely on a standard database (URW-std), with sampling from the segments discretized for flow and transport simulations [Painter and Cvetkovic, 2005], and on a modified database (URW-mod), which is defined to record the data by space-Lagrangian velocities with a fixed space lag $\Delta x'$ [Kang et al., 2019]. These methods are used in Section 3.3 to reproduce the transport behavior described in Sections 3.1 and 3.2 considering the average length 0.05 m for the standard database sampling and $\Delta x' = 0.5$ m for the modified database.

As these methods fail to reproduce some of the anomalous transport behavior provided in Section 3, we suggest two improvements of MDRW method. (i) The modified database usually considered with URW method is used with the MDRW method, leading then to the distinction between MDRW-std and MDRW-mod methods using standard and modified database, respectively. Note that in both cases, the number of velocity states is $N_{\mathrm{m}} = 10$ for the results provided in Section 3.3. (ii) We consider that the first velocity experienced by the particles, i.e., the velocity of the fracture segment in which the particle is injected, is a determinant information for the particle trajectories. From this statement, we propose an alternative method that is called Multi-M MDRW and rely on multiple transition matrices according to the initial space-Lagrangian velocities. To do this, the initial velocity probability V defining the first velocity that is associated with the particles is recorded with V_k the probability of traveling with velocity v_k. When running the Multi-M MDRW method, the initial state of the particles is determined from V and the corresponding transition matrix A_k conditioned by the initial state v_k is used to determine the next flow velocities. After

assigning the initial velocity v_k from probability V, the particles move along a 1D line with the constant spatial step $\Delta x'$ and time step $\Delta t' = \Delta x'/v_k$, and the next velocities v are defined from the correlation matrix A_k at each jump, as in the existing MDRW method. Following the formulation used for MDRW method, the successive motion distribution of Multi-M MDRW is expressed as

$$f\left(\Delta\tau_1', \Delta\tau_2', \cdots, \Delta\tau_n'\right) = \sum_{S_1 \in S} f\left(\Delta\tau_1' \mid S_1\right) P_{S_1} \sum_{S_2 \in S} f\left(\Delta\tau_2' \mid S_2\right) A_{S_1 S_2} \left| S_1 \cdots \sum_{S_n \in S} f\left(\Delta\tau_n' \mid S_n\right) A_{S_{n-1} S_n} \right| S_1 \tag{2}$$

where $f(\Delta\tau' \mid S)$ is the probability density function of $\Delta\tau'$ for a particle being at state S and P_{S_1} the probability of being at state S_1.

The impact of diffusion in the matrix domain is added to the above framework by sampling the retention time from expression (1) at every sampling of space-Lagrangian velocity v. Note that the computation of t_{diff} is simplified by considering the mean aperture of the fracture network.

3. Results

3.1. Impact of stress-induced aperture changes

Figure 2 shows the BTCs that are obtained by running the particle-tracking method described in Section 2.2 at the fracture-network scale on the domains defined in Section 2.1. Matrix diffusion is not considered yet and will be analyzed separately in Section 3.4. The fracture aperture is initially set to the constant value of 0.1 mm and heterogeneous stress-induced aperture fields are obtained for the stress scenarios described in Table 1 by applying the geomechanical model described in Section 2.1. In order to focus on the impact of the changes in aperture, the growth of new cracks is not considered in the present section and is studied in Section 3.2. The results shown in Figure 2 are normalized by the peak arrival time

of the reference zero-stress configuration, denoted *Iso1* (Table 1). Furthermore, additional results are shown in Figures 3 and 4. Figure 3 shows the changes in aperture and particle trajectories due to the stress scenarios applied to the system with (i) the mean aperture of the three major fracture sets for the different stress scenarios normalized by that of the reference case with no stress (Figures 3a-d), and (ii) contribution of the three major fracture sets to transport defined as the time spent by the particles in each fracture set normalized by the time spent in all fracture sets. The contribution to transport is also normalized by that of the reference case (Figures 3e-h). Finally, Figure 4 shows the spatial distribution along the outlet border (right border) of the proportion of particles exiting the system for different anisotropic-stress cases. Note that we discuss here the impact of the different stress scenarios and orientation on the transport behavior. The reader can refer to Jiang et al. [2019] for an analysis of the fracture length and orientation and their impact on the BTCs.

Applying the isotropic stress condition *Iso2* results in a simple delay in the arrival times of particles in comparison with the reference case *Iso1* without stress condition (Figure 2). The shapes of the curves are similar (from orange to green curves), which is consistent with the observations made in previous studies [Zhao et al., 2011, Kang et al., 2019]. This is because the closure in the fracture aperture under isotropic stress is controlled by normal compression while the shearing effect is negligible [Jiang et al., 2019]. This is also shown in Figure 3 where we observe that the mean aperture $\bar{b}$ uniformly decreases over the three major fracture sets when applying isotropic stress (*Iso2*), since we observe the same value of $\bar{b}$, that is smaller than 1, for the fracture sets 5°, 50° and 120° for all the considered configurations of stress orientation (green curves in Figures 3a-d). This results in no changes in the contribution of the main fracture sets to transport (the same value of $\sim$1 for all fracture sets, green curves in Figures 3e-h) and explains the overall delay observed in the BTCs for case *Iso2*. Note that the shape of BTCs exhibits a Gaussian-like distribution, which is similar to the

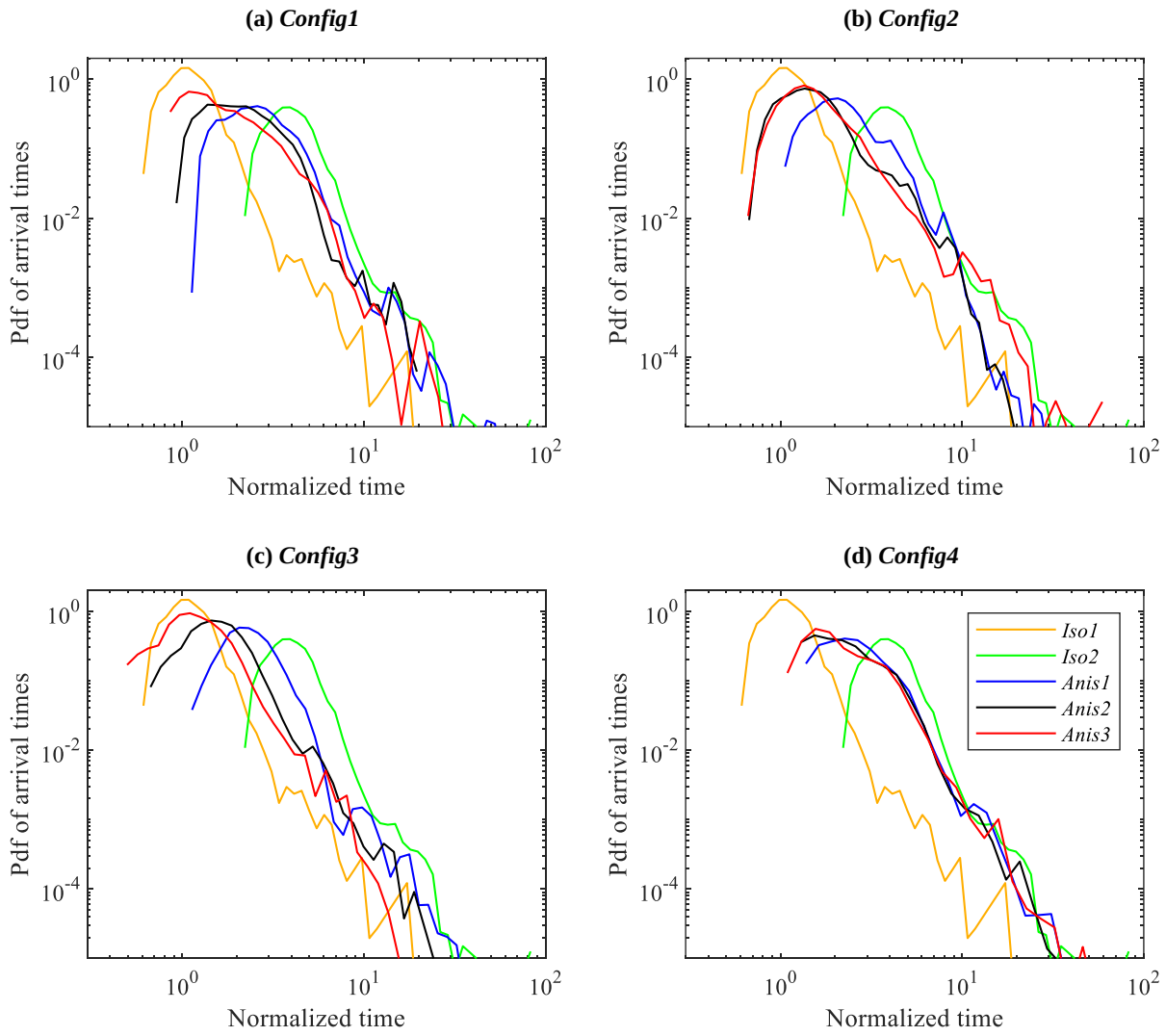

Figure 2: Breakthrough curves for the stress scenarios described in Table 1 without stress-driven crack growth and for the stress loading directions considered in (a) *Config1* ($\theta = 50°$), (b) *Config2* ($\theta = 80°$), (c) *Config3* ($\theta = 120°$) and (d) *Config4* ($\theta = 150°$).

observation in Kang et al. [2019]. This indicates that the geometrical heterogeneity of the fracture network is not sufficient to produce anomalous transport as the aperture is uniform for the no-stress case (also similar for the isotropic-stress case). It is also consistent with the distribution of emitted particles shown in Figure 4 where the preferential outlet (Y=-2.79 m) is not very pronounced (below 0.2) and secondary outlets emit an important proportion of particles (black bars in Figure 4).

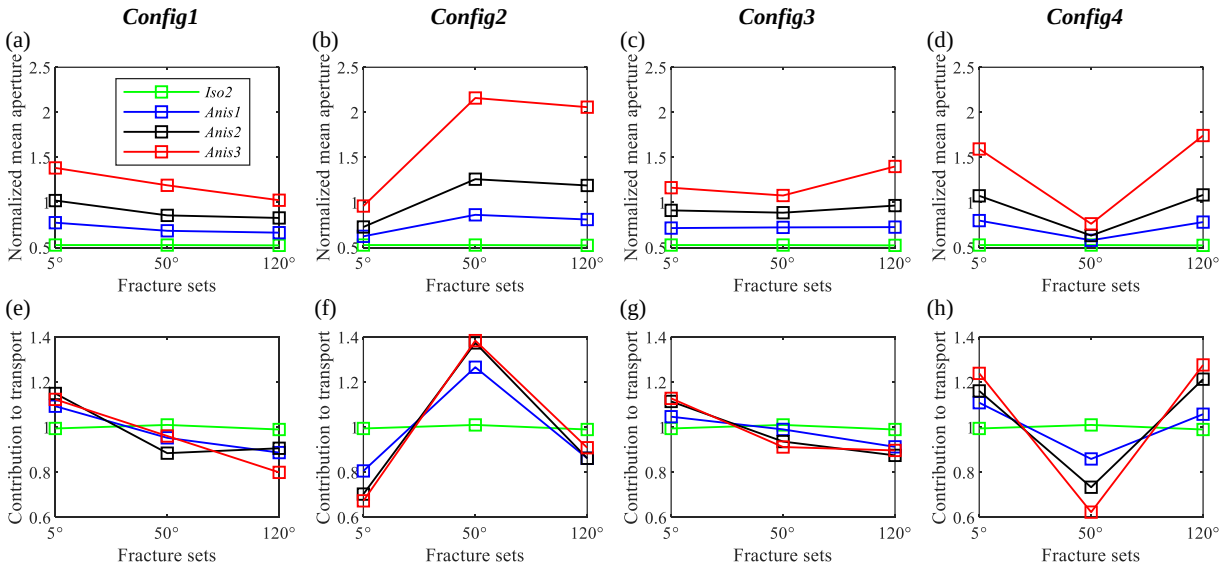

Figure 3: First row: mean aperture $\bar{b}$ of the three major fracture sets (5°, 50°, and 120°) under the stress conditions described in Table 1 and normalized by that of the reference case. Second row: contribution of the three major fracture sets to transport defined as the time spent by the particles in each fracture set normalized by the time spent in all fracture sets. The contribution to transport is also normalized by that of the reference case.

Applying anisotropic stress conditions (*Anis1*, *Anis2*, and *Anis3*) results in broader arrival time distributions with earlier arrival times (from green to blue, black and red curves in Figure 2), which is attributed to local permeability enhancement by shearing [Zhao et al., 2011, Kang et al., 2019]. Shearing impact is visible on the changes in aperture and transport trajectories shown in Figure 3 where we observe non-uniform changes for all the anisotropic cases, except for *Anis1* and *Anis2* in *Config1* and *Config3*. In the latter cases, shearing on the fracture sets tends to be suppressed since $\bar{b}$ varies from 0.6 to about 1 (from blue to black curves in Figures 3a and c). This is explained by the stress loading directions that are aligned with one of the major fracture sets in *Config1* and *Config3* while the three fracture sets tend to have large normal stress or small shear stress, which makes difficult to activate shearing and dilatancy. On the contrary, increasing the loading stress from *Anis2* and *Anis3*, or considering other configuration scenarios (*Config2* and *Config4*), results in heterogeneous changes in fracture apertures and transport behavior depending on the fracture orientation.

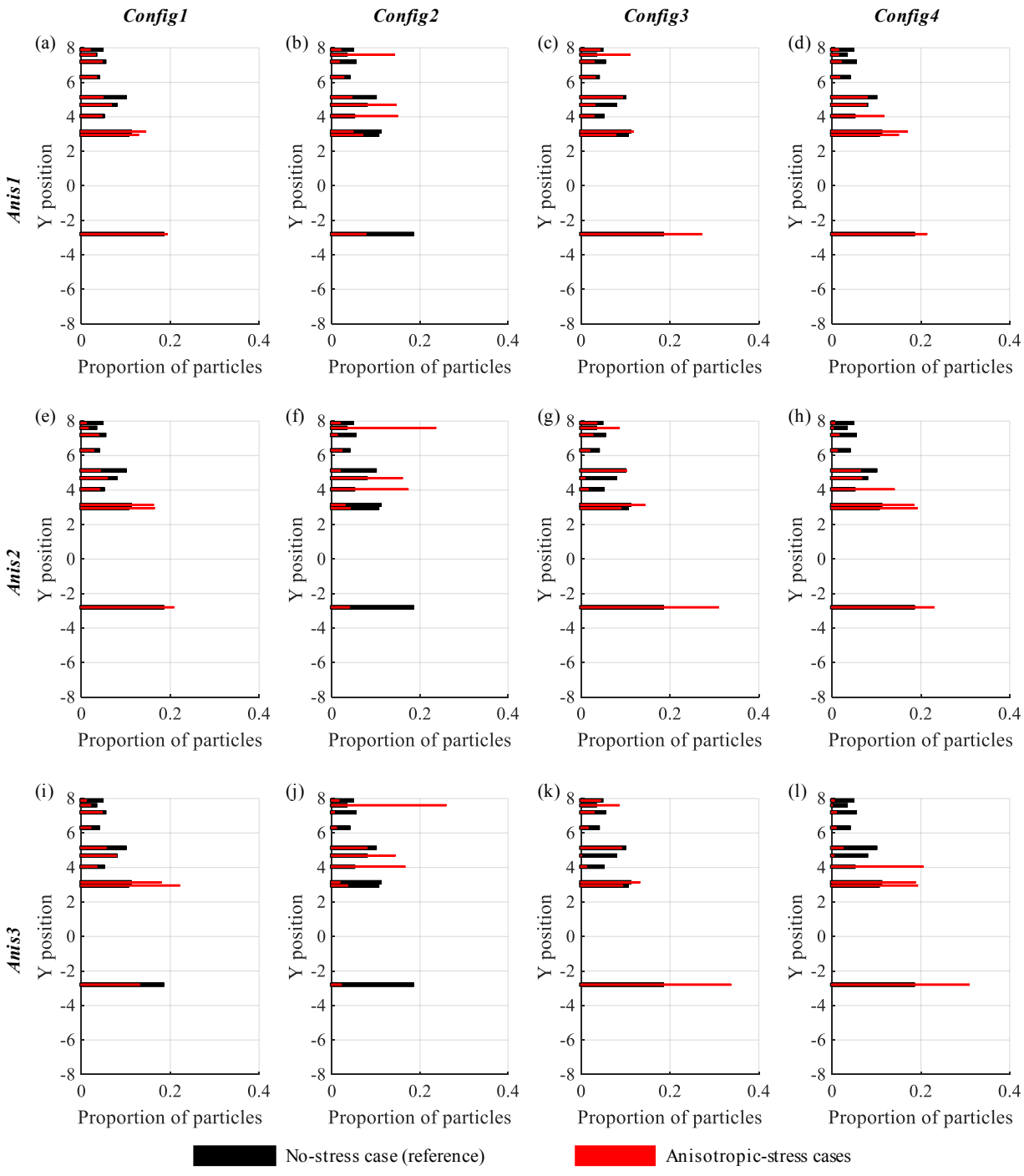

Figure 4: Spatial distribution along the outlet border (Y position from -8 to 8) of the proportion of particles exiting the system for different anisotropic-stress cases without stress-driven crack growth.

Different transport behaviors are also shown by the distribution of emitted particles at the outlet boundary (Figure 4). We observe for example in *Config2* that there is not a main preferential outlet for small stress ratio (*Anis1*, Figure 4b), while a new preferential outlet is created when increasing the stress ratio from *Anis1* to *Anis2* (Figure 4f) with no significant changes from *Anis2* to *Anis3* (Figure 4j). This explains the different behavior observed in the BTCs in Figure 2b between *Anis1* and *Anis2*, and the similar behavior between *Anis2* and *Anis3*. We also observe that in some cases, the preferential outlet observed for the no-stress reference case (Y=-2.79 m) is greatly enhanced (*Config3* in Figures 4c, g and k), and in other cases some secondary channels become stronger (*Config1* in Figures 4a, e and i), resulting in different behavior in the corresponding BTCs where anomalous transport behavior emerges with early arrival times (Figures 2a and c). Finally, for the cases related to *Config4*, both the no-stress preferential outlet and the secondary outlets are enhanced when increasing the stress ratio (Figures 4d, h and l), explaining that no significant changes are observed in the corresponding BTCs (Figure 2d).

3.2. Effect of stress-driven crack growth

As the anisotropic stress loadings tend to drive the formation of new cracks due to stress concentration at the tips of pre-existing fractures [Jiang et al., 2019], we further examine the effect of stress-driven crack growth on transport behaviors. As confirmed in Figure 5 and shown in Jiang et al. [2019], isotropic stress loading do not generate new crack growth, implying that we study only the cases of anisotropic stress loadings by comparing the breakthrough curves between the cases without and with new cracks (Figure 6). We also compare the changes in flow velocities and particle trajectories (Figure 7), as well as in outlet spatial distribution (Figure 8). Note that there are no changes in the normalized mean aperture between the configurations without and with new cracks, implying that these results are not shown.

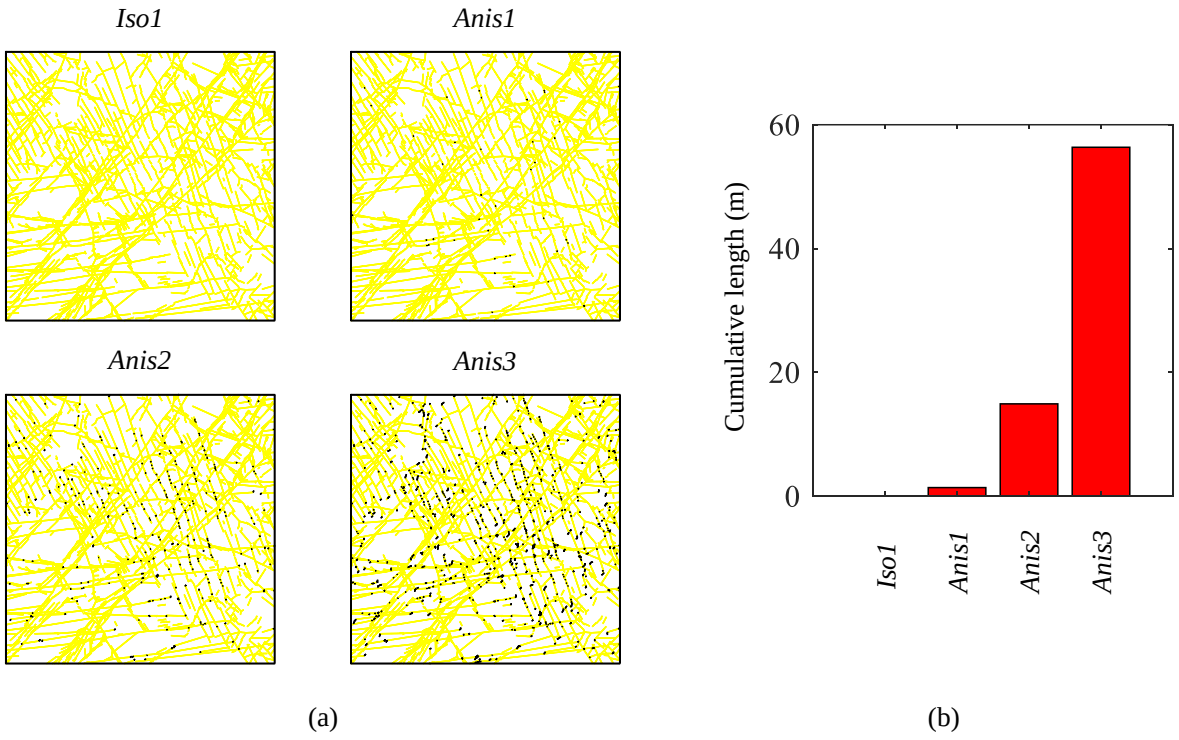

Figure 5: (a) Resulting fracture networks composed of the pre-existing fractures and new cracks (yellow and black lines, respectively) and (b) cumulative length of new cracks for the stress configuration *Config1* and the stress scenarios presented in Table 1.

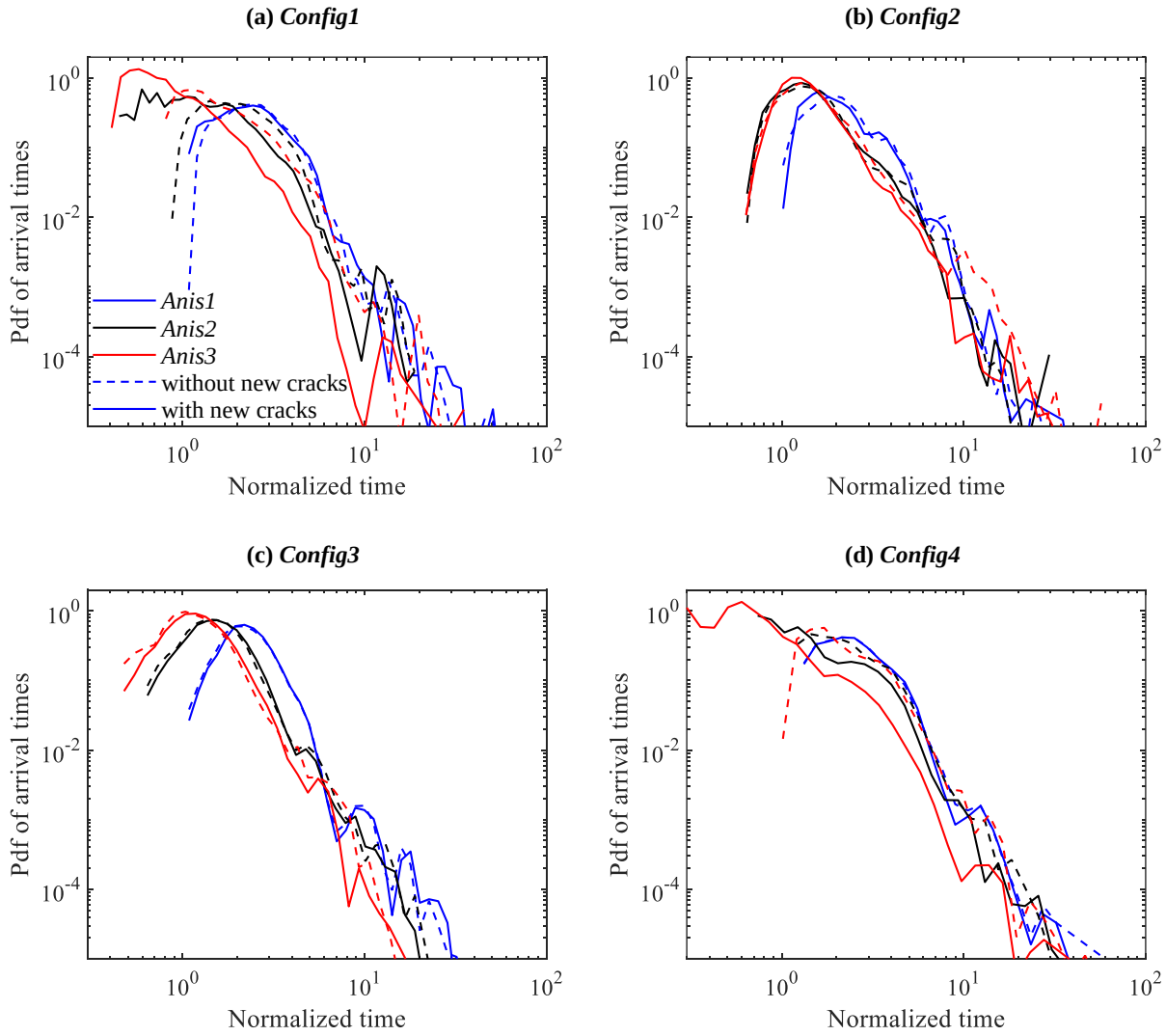

Figure 6: Comparison of breakthrough curves without and with (dashed and solid lines, respectively) new cracks for various anisotropic-stress cases.

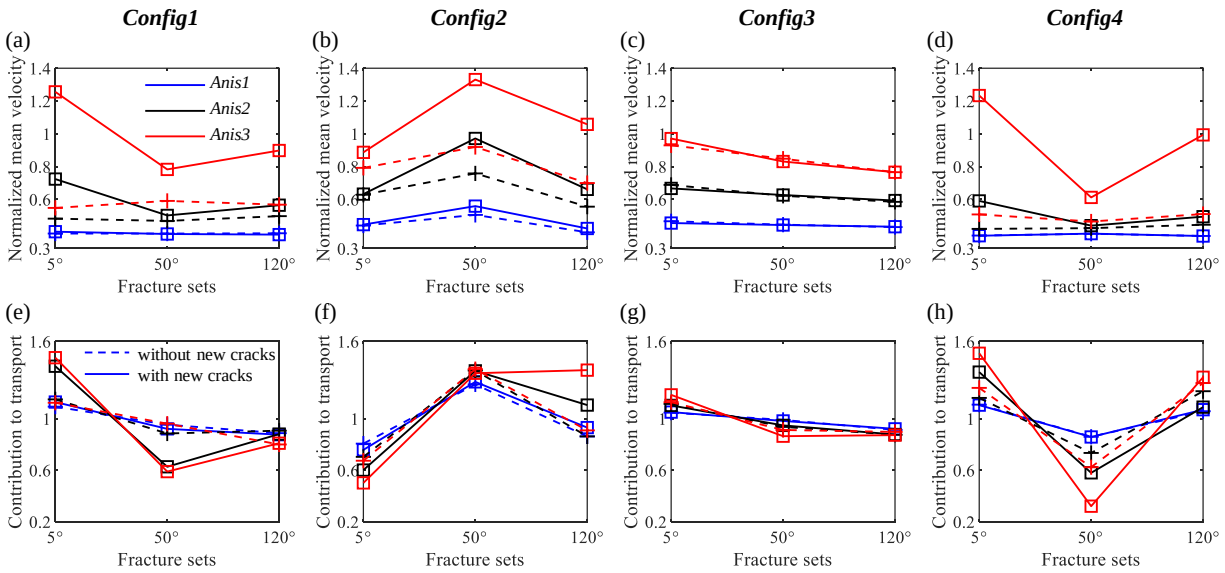

Figure 7: First row: mean velocity $\bar{v}$ of the three major fracture sets (5°, 50°, and 120°) under the differential stress conditions *Anis1*, *Anis2*, and *Anis3* that are normalized by that of the reference case. Second row: contribution of the three major fracture sets to transport defined as the time spent by the particles in each fracture set normalized by the time spent in all fracture sets. The contribution to transport is also normalized by that of the reference case.

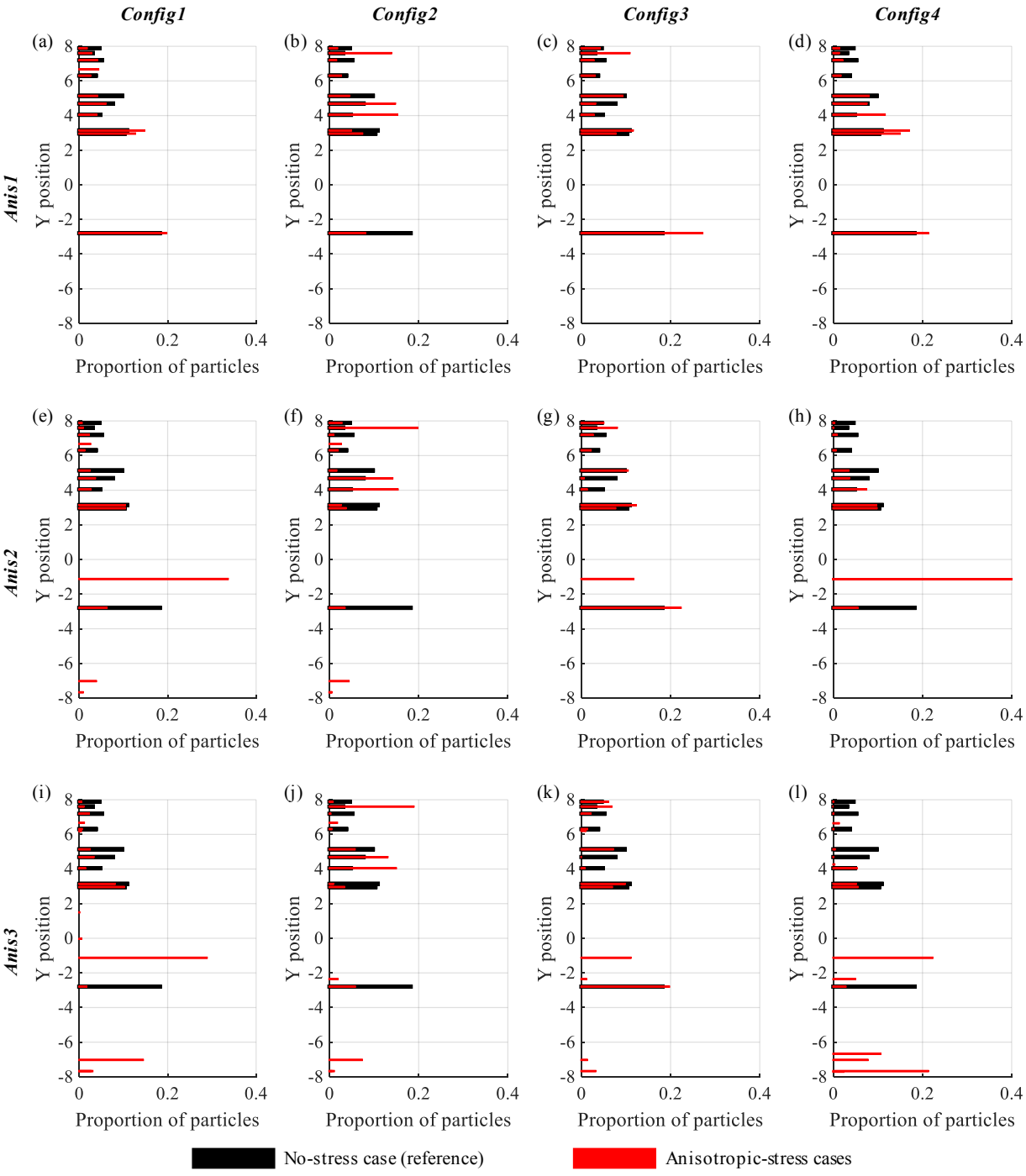

Figure 8: Spatial distribution along the outlet border (Y position from -8 to 8) of the proportion of particles exiting the system for different anisotropic-stress cases with stress-driven crack growth.

The results presented in Figure 6 show that the number of new cracks created with

scenario *Anis1* is too small to impact the transport behavior since the results without and with new cracks are similar for this case (blue curves in Figure 6). This is confirmed by the normalized mean velocity and contribution to transport that are similar for the configurations without and with new cracks with scenario *Anis1* (blue curves in Figure 7). For this scenario, we also observe no significant changes in the spatial distributions of particles exiting the system between the configurations without new cracks (Figures 4a-d) and that considering the effect of new crack growth (Figures 8a-d).

For scenarios *Anis2* and *Anis3*, the impact of new cracks on transport depends on the loading configurations. For *Config3*, similar results are observed between the systems without and with new cracks (Figure 6c), while changes in late arrival times are observed for *Config2* and *Anis3* (red curves in Figure 6b). For *Config1* and *Config4*, changes in early arrival times are observed with *Anis2* and over all the arrival times with *Anis3* (black and red curves in Figures 6a and d, respectively). These observations are well explained by the results shown in Figures 7 and 8. For *Config3*, we observe no significant changes in the normalized mean velocity and contribution to transport of the three main fracture sets (Figures 7c and g), and the changes in the proportion of particles along the outlet border are restricted to either slightly enhancement of existing main paths (e.g., Y=-2.79 m in Figures 8g and k) or new paths that do not have a significant impact with a proportion of particles smaller than 0.2 (e.g., Y=-1.12 m in Figures 8g and k). Similar changes in the spatial distribution of the particles exiting the systems are observed for *Config2* (Figures 8f and j), with larger values of mean velocity when considering new cracks (Figure 7b) and a larger contribution to transport of the fracture set 120° (Figures 7f), resulting in the larger late arrival times observed in the BTCs for *Anis3* (red curve vs. blue curve in Figure 6b). Finally, the smaller early arrival times observed with *Anis2* for *Config1* and *Config4* are related to the creation of new main preferential paths that have a strong impact on the transport organization with a proportion of particles exiting the system from these paths

larger than 0.3, these paths being located at position Y=-1.12 m for both configurations, respectively (Figures 8e and h, respectively). However, the changes in mean velocity and contribution to transport over the whole system are not significant (black lines in Figures 7a and e for *Config1* and Figures 7d and h for *Config4*), implying that only early arrival times are impacted by this stress scenario. Alternatively, when applying stress scenario *Anis3*, the changes in flow velocity and contribution to transport are significant (red lines in Figures 7a and e for *Config1* and Figures 7d and h for *Config4*), and the new outlets at the bottom are strengthened while the new preferential outlets in the middle are weakened (Figures 8i and l). Smaller arrival times over the full range of particle arrival times are then observed (red curves in Figures 6a and d) with a less uniform distribution of emitted particles at the outlet boundary compared to the cases without new cracks. This results in anomalous transport behavior where the propagation of new cracks generates BTCs with multiple peaks.

3.3. Upscaling of transport properties

In this section, we use a series of upscaling methods based on the random walk theory to capture the transport behavior under various stress conditions. Traditional methods (i.e., URW and MDRW) are first applied to examine their predictive performance. To this end, we compare the three existing methods URW-std, URW-mod, and MDRW-std that are described in Section 2.3. Figures 9 and 10 show the results of upscaling of the small-scale transport behavior shown in Figures 2 and 6 without and with new cracks, respectively. All the configurations and stress scenarios presented in Section 2.1 are considered. Note that the results obtained for scenarios *Iso1* and *Iso2* are only shown once (Figures 9a-b) since the results are the same for the four considered stress configurations and the cases without and with new cracks. Furthermore, to quantify the performance of different upscaling methods, the statistics of mean, standard deviation, and skewness of each breakthrough curve [Schiavo et al., 2022] are shown in Figure 11. The skewness is defined as $\gamma = E\left[\left(\frac{x-\mu}{\sigma}\right)^3\right]$ where E

is mathematical expectation, μ and σ are respectively the mean and standard deviation of variable x. Here $x = \log_{10}(t)$ where t is the normalized time in Figures 9 and 10.

The results presented in Figures 9, 10 and 11 show that the method URW-std (dashed blue curves) never succeeds in reproducing the transport behavior observed with the direct small-scale simulations (solid black lines), because the intrinsic correlation between successive velocity samplings is not considered with this method. Changing the database used by URW (URW-mod, dashed green lines) or introducing a velocity correlation with MDRW method (MDRW-std, dashed red lines) help to reproduce well the reference simulations for isotropic cases (Figures 9a-b, Figures 11a-c). Consequently, if the sampling database is modified by space-Lagrangian velocities, the performance of the URW method is greatly improved, with results that are similar to that of the MDRW method with the standard database (Figure 11). This is because the modified database with URW includes the correlation information within the distance of the large sampling lag (0.5 m) compared to the standard database with a small segment discretization (0.05 m). However, for anisotropic-stress cases, both URW-mod and MDRW-std do not reproduce well the small-scale results due to the shearing-induced anomalous transport phenomenon that is hard to reproduce (Figures 9 and 11a-c), this issue being even worse when considering cases with new cracks for which the anomalous transport behavior is more pronounced and thus harder to reproduce (Figures 10 and 11d-f). This is consistent with previous studies showing that traditional upscaling framework that only considers the average correlation property is likely to fail in fracture systems driven by shear dilation-induced preferential flow paths [Kang et al., 2019].

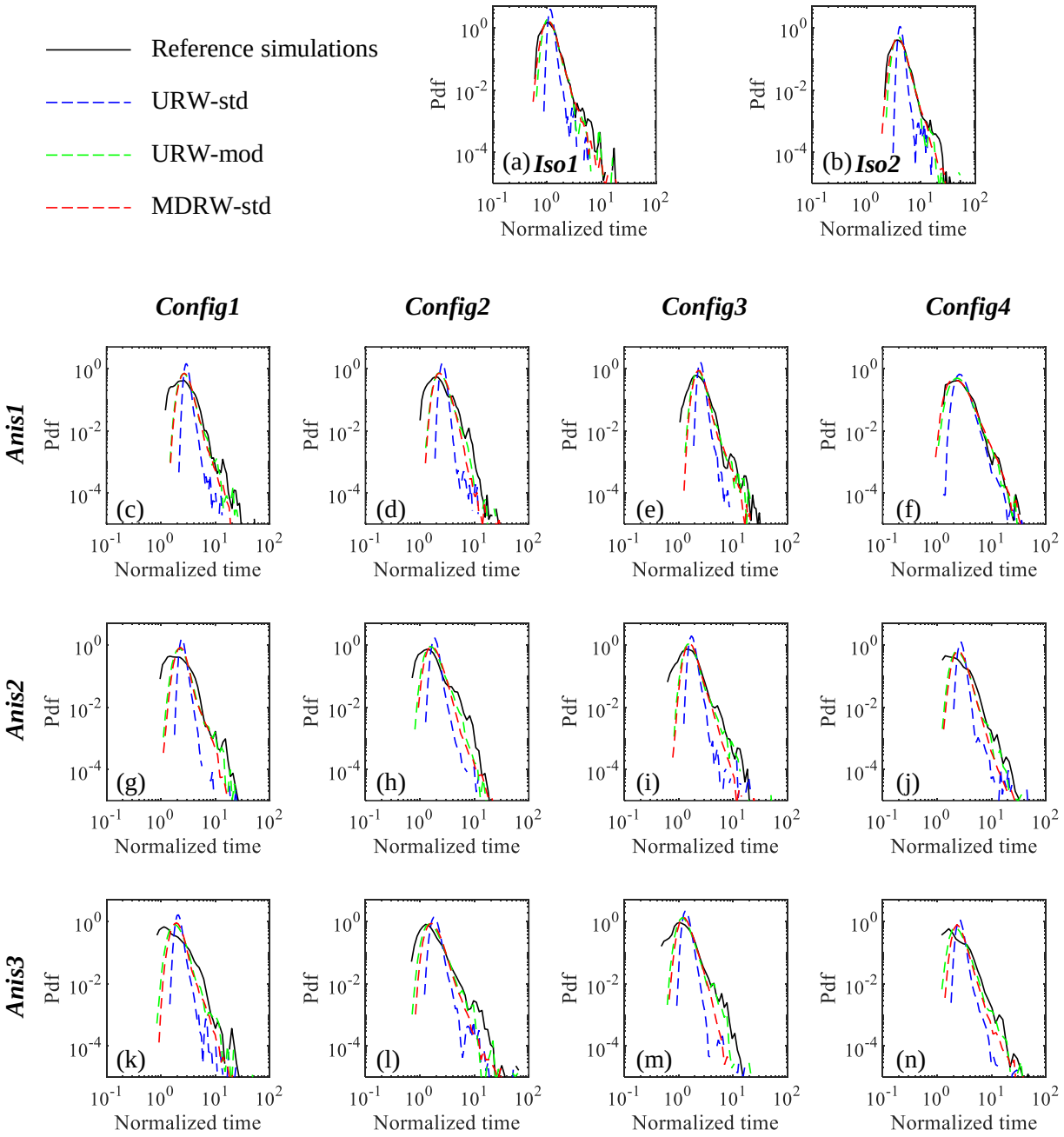

Figure 9: Breakthrough curves from reference small-scale simulations (solid black line) and upscaled model predictions (dashed lines) using URW-std, URW-mod, and MDRW-std methods (dashed blue, green, and red curves, respectively) without considering the effect of new crack propagation.

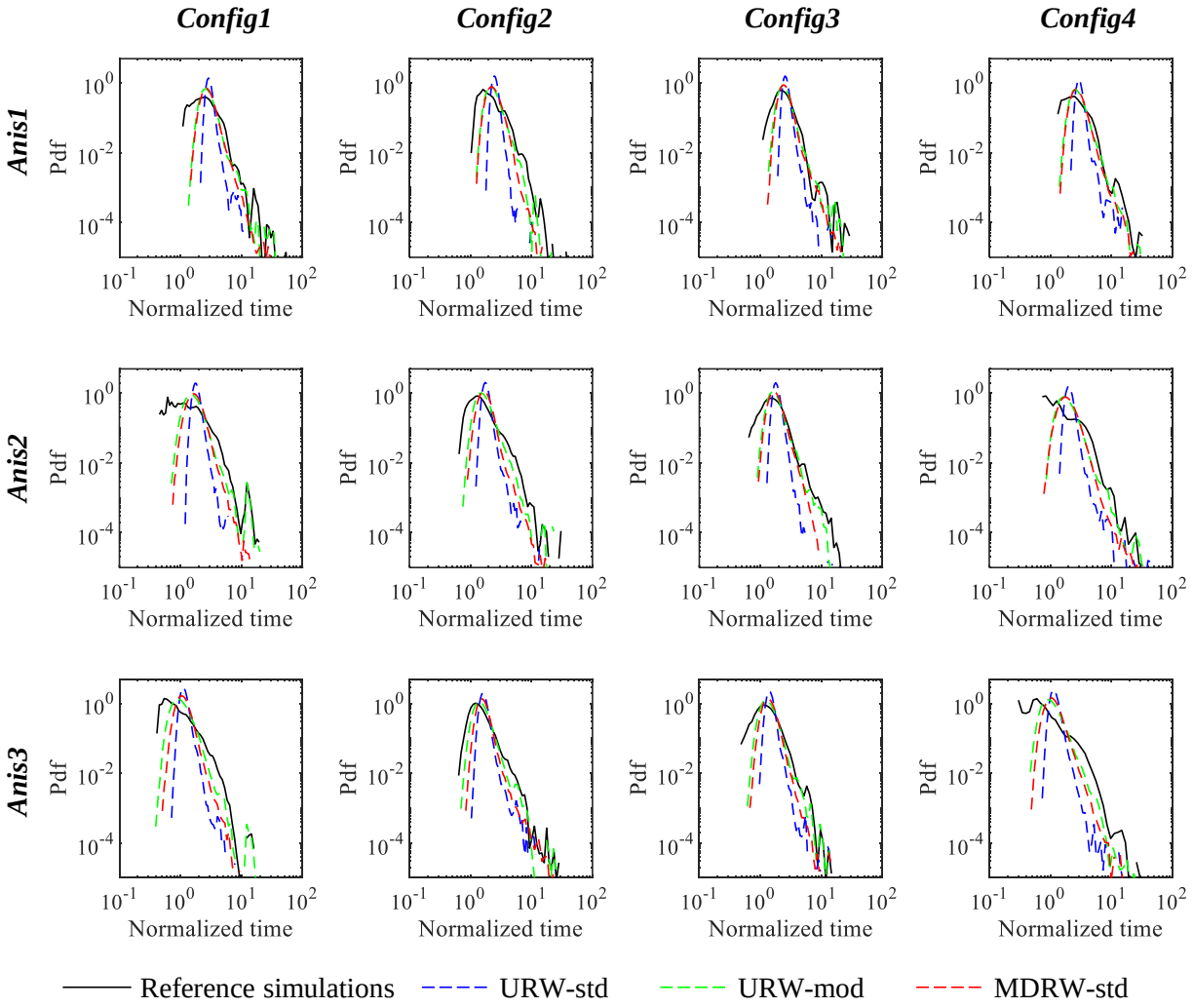

Figure 10: Breakthrough curves from reference small-scale simulations (solid black line) and upscaled model predictions (dashed lines) using URW-std, URW-mod, and MDRW-std methods (dashed blue, green, and red curves, respectively) considering the effect of new crack propagation.

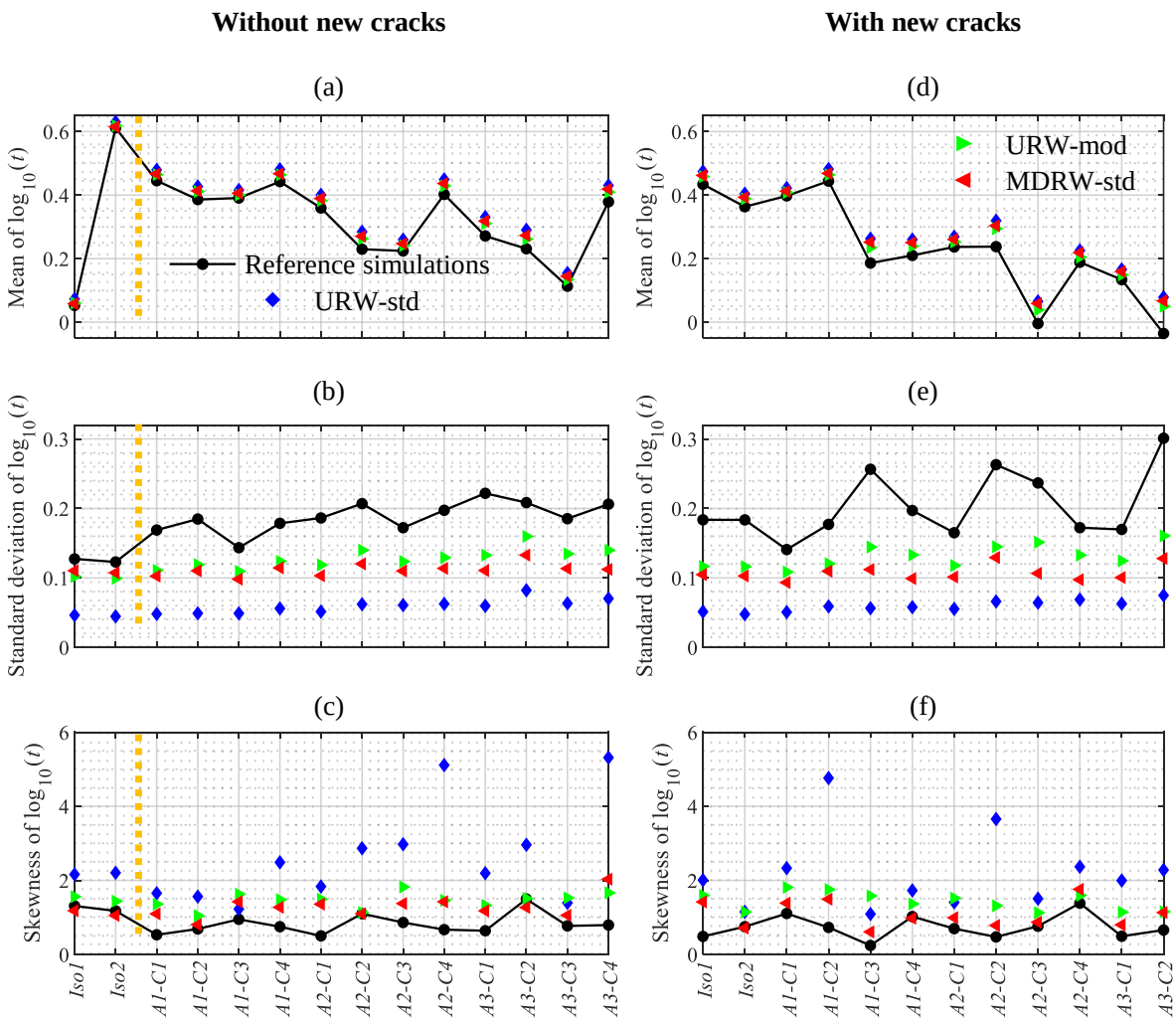

Figure 11: Statistics of mean, standard deviation and skewness of $\log_{10}(t)$ where t is the normalized time in Figures 9 and 10.

To overcome this issue, we attempt to improve the predictive performance of traditional upscaling methods with the modified methods MDRW-mod and Multi-M MDRW. The corresponding results are shown in Figures 12 and 13 with the quantitative statistics in Figure 14. We observe that, after adding the velocity correlation between the samplings of space-Lagrangian velocities, the modified MDRW method is able to well capture the majority of the cases in this study. Compared to the MDRW with the standard database, the performance of MDRW with the modified database is greatly improved, which highlights

the importance of space-Lagrangian velocities. Both MDRW-mod and Multi-M MDRW provide satisfying results to reproduce the BTCs obtained at the fracture-network scale. In some cases, the Multi-M MDRW method is better suited to reproduce the complex behavior observed at the beginning of the curves. This is the case for example in the highly heterogeneous cases *Config4-Anis3* without and with new cracks (Figures 12n and 13n), for which the information of the first velocity experienced by the particles (that is included in the Multi-M MDRW method) is an information for the particle trajectories. From the quantitative statistics in Figure 14, it is more pronounced that results from Multi-M MDRW almost overlap the reference cases, especially for the standard deviation of $\log_{10}(t)$, which indicates a better performance than MDRW.

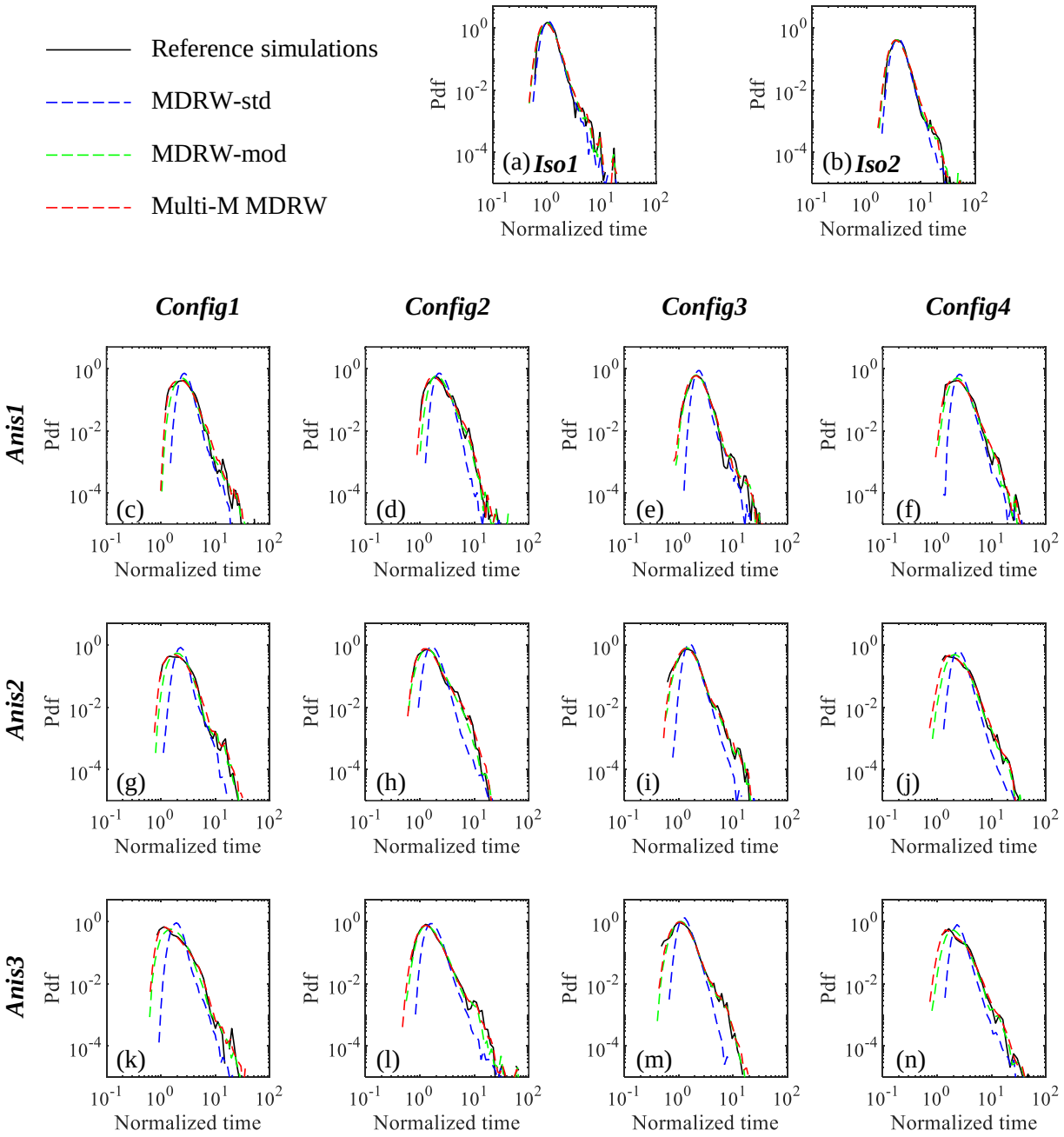

Figure 12: Breakthrough curves from reference small-scale simulations (solid black line) and upscaled model predictions (dashed lines) using MDRW-std, MDRW-mod, and Multi-M MDRW methods (blue, green, and red, respectively) without considering the effect of new crack propagation.

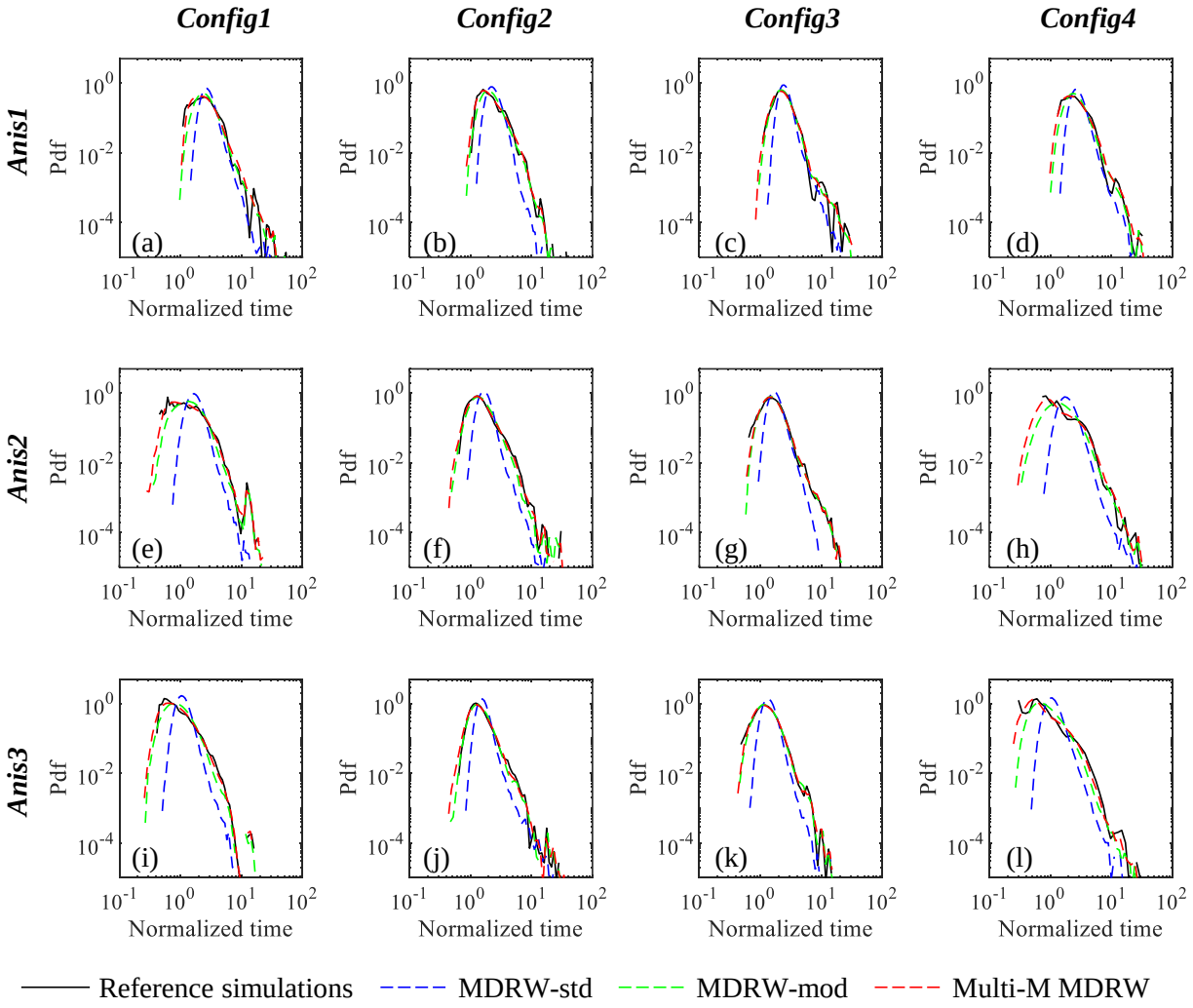

Figure 13: Breakthrough curves from reference small-scale simulations (solid black line) and upscaled model predictions (dashed lines) using MDRW-std, MDRW-mod, and Multi-M MDRW methods (blue, green, and red, respectively) considering the effect of new crack propagation.

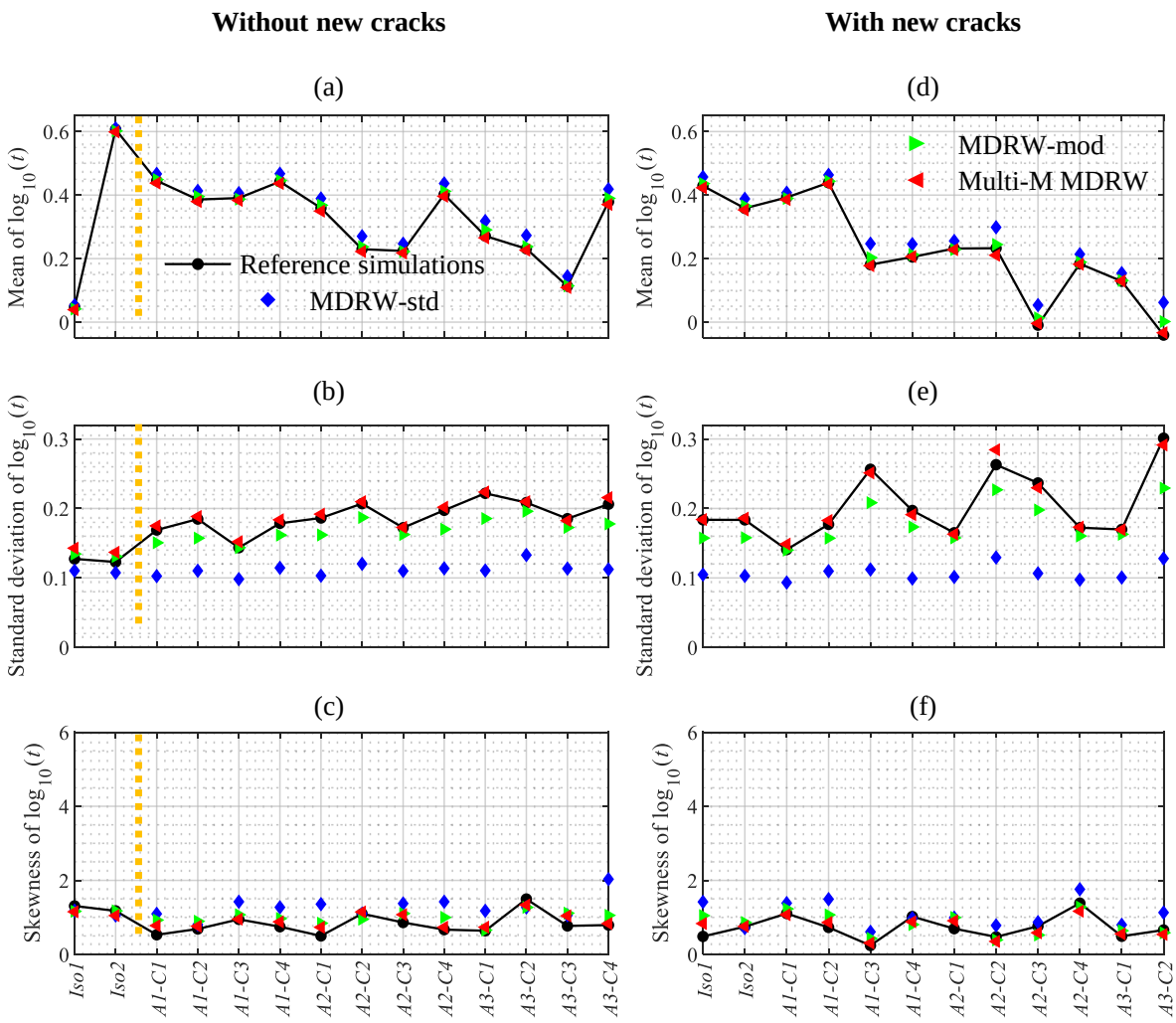

Figure 14: Statistics of mean, standard deviation and skewness of $\log_{10}(t)$ where t are the normalized time distributions corresponding to Figures 12 and 13.

3.4. Effect of diffusion transport in rock matrix

We wish now to test the upscaled models previously presented in the context of both advective and diffusive processes in the fractures and matrix, respectively. To this end, we consider equation (1) to define the matrix diffusion time in both direct and upscaled simulations. Figures 15 and 16 show the breakthrough curves obtained for the stress configurations and scenarios previously defined with the direct small-scale simulations (solid black curves) and the MDRW-mod and Multi-M MDRW upscaled models (dashed blue and red

lines, respectively) without (Figure 15) and with (Figure 16) considering the effect of new crack propagation. In Figure 17, the quantitative statistics show that, as expected, matrix diffusion results in long tails of the breakthrough curves with a fixed slope of -1.5 that corresponds to pure diffusion process. Considering matrix diffusion tends to homogeneize the results with similar curves for the different considered stress scenarios. Compared to the cases without matrix diffusion (Figures 2 and 6), the early part of the curves is smoother and do not present multi-peak behavior as before for the most heterogeneous cases (*Config4-Anis2* and *Config4-Anis3*). The two upscaling methods reproduce well the considered BTCs with small differences for the early arrival times in some cases where the Multi-M MDRW method provides a better fit than the MDRW method. For these cases, the better representation of the initial velocities investigated by the particles plays an important role in simulating the early arrival times, since the matrix diffusion time directly depends on the advective times (expression (1)). This confirms the effectiveness of the Multi-M MDRW method in upscaling stress-induced anomalous transport behavior for various configurations in terms of stress scenarios and considered processes.

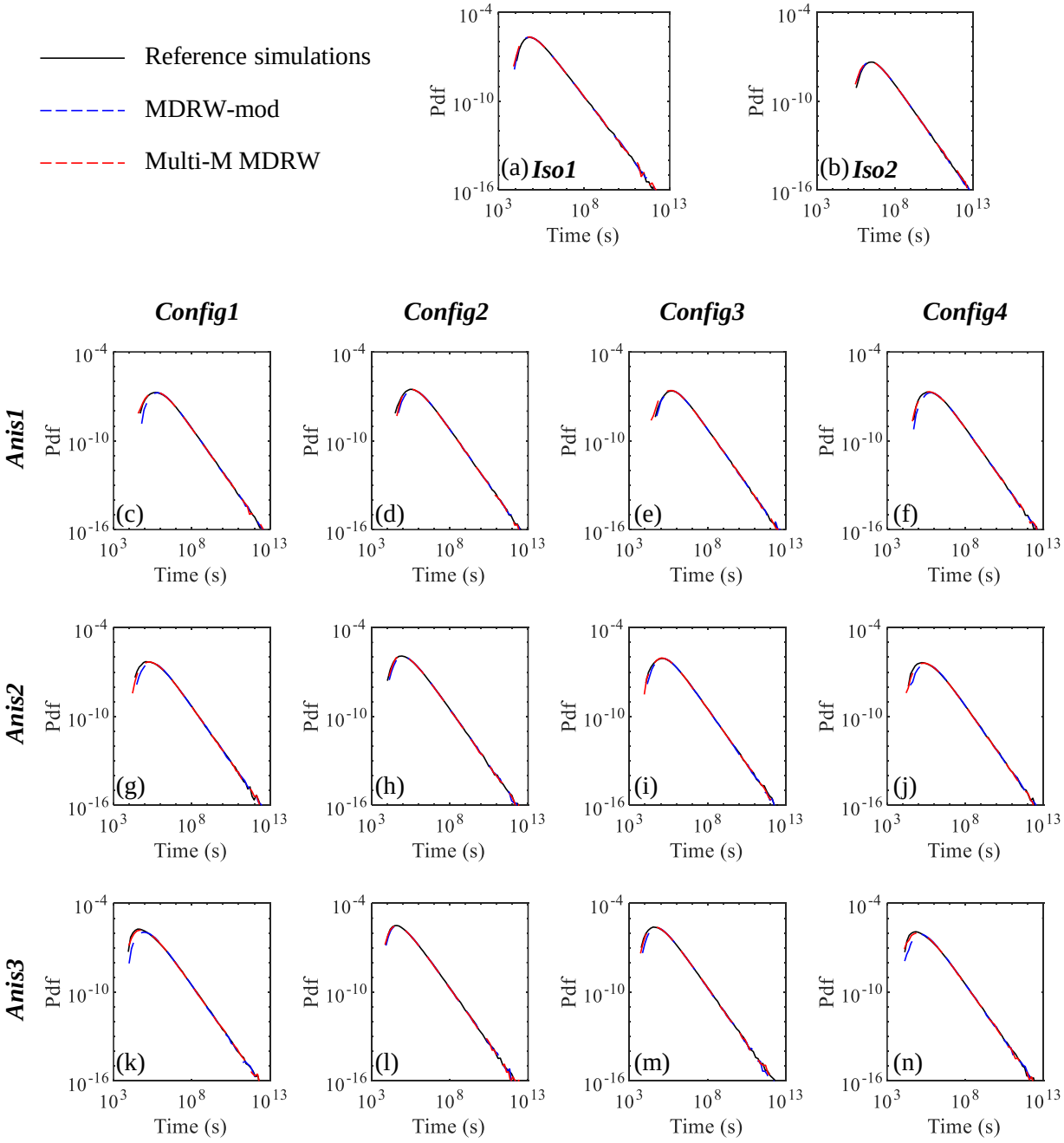

Figure 15: Breakthrough curves from the direct numerical simulations with matrix diffusion (black solid line) and upscaled model predictions using MDRW-mod and Multi-M MDRW methods with matrix diffusion (dashed blue and red lines, respectively) without considering the effect of new crack propagation.

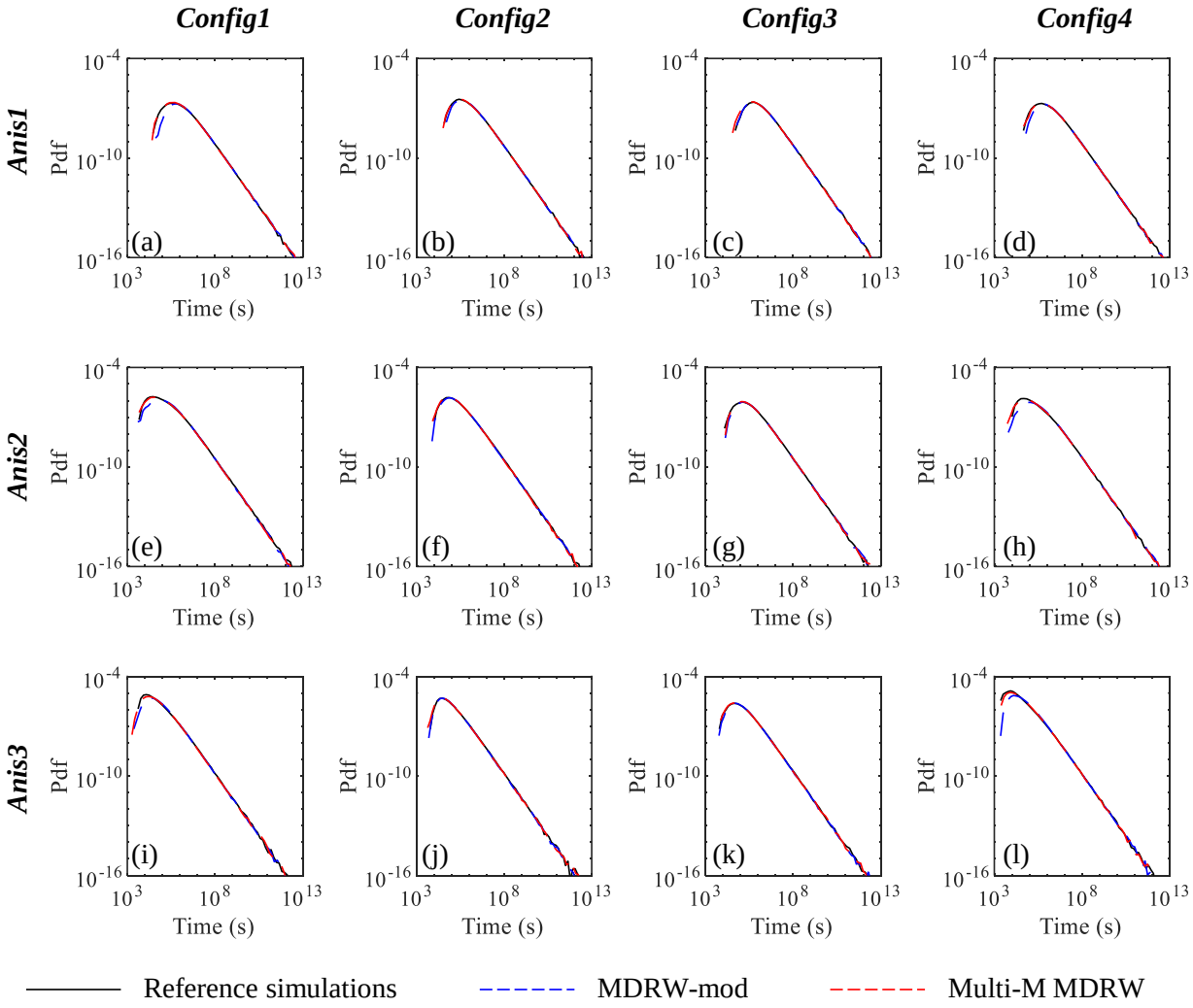

Figure 16: Breakthrough curves from the direct numerical simulations with matrix diffusion (black solid line) and upscaled model predictions using MDRW-mod and Multi-M MDRW methods with matrix diffusion (dashed blue and red lines, respectively) considering the effect of new crack propagation.

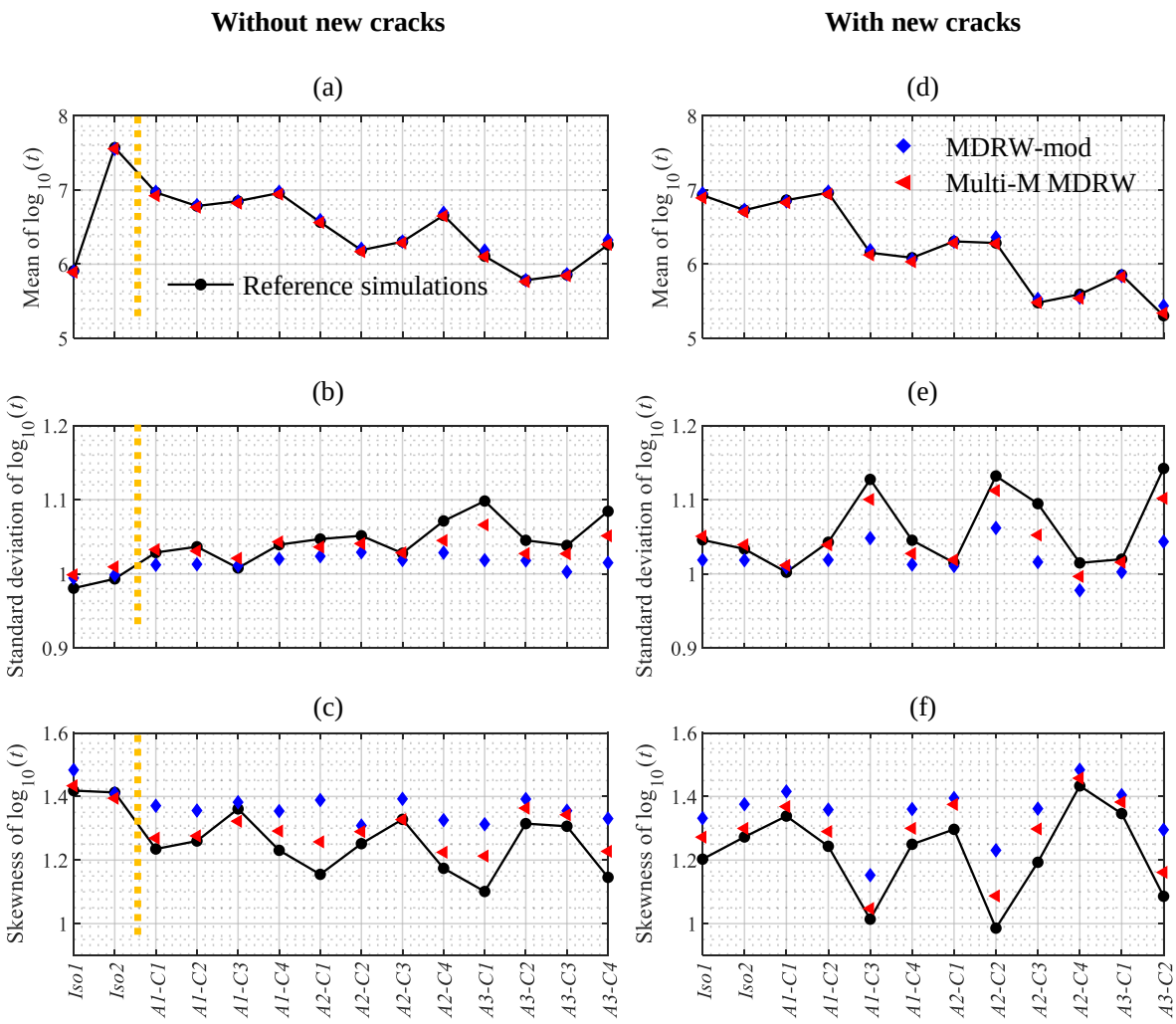

Figure 17: Statistics of mean, standard deviation and skewness of $\log_{10}(t)$ where t are the normalized time distributions corresponding to Figures 15 and 16.

4. Discussion and conclusions

In this paper, we evaluate the impact of various stress scenarios on transport behaviors in critically-connected fractured rocks with three main fracture sets. Various stress orientations and a large range of stress ratios between the maximum and minimum principal stress strengths are studied, and both traditional and improved upscaling methods are considered to determine their applicability to such stress-induced transport behaviors. Under isotropic

stress conditions, the changes over the whole system tend to be uniformly distributed, and the breakthrough curves are simply shifted from the reference results without stress. In such conditions, transport behaviors usually exhibit a Gaussian-like distribution, that is well captured by traditional upscaling methods with space-Lagrangian velocities description. Under anisotropic stress conditions, stress-induced transport exhibits broader arrival time distributions with different behavior depending on the stress orientation and strength. This is consistent with existing studies showing that the anomalous behavior featured by the early arrival times may be not pronounced under some stress orientations because the major compressive principal stress is perpendicular to the flow direction, suppressing and altering the preferential flow paths [Sweeney and Hyman, 2020]. This differs from the case of a ladder-shape fracture network topology, where the anisotropic stress orientation is along the through-going long fractures and exhibits a breakthrough behavior similar to the no-stress and isotropic-stress cases [Kang et al., 2019]. The behaviors observed in our study are enhanced when considering the effect of new crack growth that is observed under anisotropic stress loading and for high-stress ratio and some stress orientations, leading to strong anomalous phenomenon with multi-peak BTCs.

In terms of upscaling representation, it is necessary to integrate the space-Lagrangian velocities description with a large sampling distance to improve the performance of traditional methods. The proposed modified MDRW method accurately predicts the transport behavior under low-stress ratio conditions while improvement might be required for some cases of high-stress ratio due to the strong anomalous transport phenomenon characterized by multi-peak early-times BTCs. The single transition matrix representation, which describes the average features of velocity correlation over the entire system, is extended to multiple transition matrix representations that are conditioned by the initial velocity states of the particles. (i.e., Multi-M MDRW). The resulting Multi-M MDRW successfully captures the solute transport behaviors for all the considered cases including complex combined effects of

shear dilation and crack propagation in the system, as well as the impact of diffusive transport in the rock matrix. Incorporating information related to the first velocities experienced by the particles is critical to well reproduce the early arrival times, and might be critical for future work on upscaling methods applied to reactive transport [Ding et al., 2013, Painter et al., 2008, Roubinet et al., 2022].

It is important to emphasize that the insights provided in this work are restricted to the deterministic geometry that was determined from a real outcrop. Since an accurate representation of the fracture network is not feasible in most subsurface cases, future work should focus on several realizations of networks with identical statistical properties in order to evaluate the uncertainty of our results in relation with the uncertainty of the system properties. Our recent study based on statistically generated fracture networks also found that the critically connected fracture networks have a significant alternation of heat recovery efficiency with the increase of stress load difference [Sun et al., 2020]. This may also highlight the important role of crack growth on transport behaviors in terms of statistically generated fracture networks. Another limitation of our work is the consideration of two-dimensional scenarios. Although our study regarding the geomechanical deformation of three-dimensional fractured rocks has suggested that 2D analysis may provide some indicative approximations [Lei et al., 2017b], 2D modeling certainly cannot fully represent the polyaxial geomechanical behaviors of 3D fractured rocks. Future work should focus on 3D fractured rocks and on evaluating the error induced by considering 2D domains. However, working on 3D fractured networks requires to solve computational cost issues which limit the number of fractures that can be considered so far.

5. Acknowledgments

Chuanyin Jiang is supported by the China Scholarship Council (CSC) from the Ministry of Education of P.R. China (No. 202006450151). This work was funded by PRC-CNRS Joint

Research Project from the National Natural Science Foundation of China and the French National Centre for Scientific Research (Grant no. 5181101856) obtained by Xiaoguang Wang and Delphine Roubinet, and Xiaoguang Wang was also funded by National Key Research and Development Program of China (Grant no. 2020YFC1808300), National Natural Science Foundation of China (Grant No. 42102300), Science and Technology Department of Sichuan Province (Grant Nos. 2021ZYCD004, 2022YFSY0008) and State Key Laboratory of Geohazard Prevention and Geoenvironment Protection (Grant No. SKLGP2022K024). Qinghua Lei is grateful for the support from the Swiss National Science Foundation (Grant No. IZLCZ0_189882).

References

Baghbanan, A., Jing, L., 2008. Stress effects on permeability in a fractured rock mass with correlated fracture length and aperture. International Journal of Rock Mechanics and Mining Sciences 45 (8), 1320–1334, publisher: Elsevier.

Bear, J., 2013. Dynamics of fluids in porous media. Courier Corporation.

Berkowitz, B., 2002. Characterizing flow and transport in fractured geological media: A review. Advances in Water Resources 25 (8–12), 861–884.

Berkowitz, B., Bour, O., Davy, P., Odling, N., 2000. Scaling of fracture connectivity in geological formations. Geophysical Research Letters 27 (14), 2061–2064.

Berkowitz, B., Scher, H., 1997. Anomalous transport in random fracture networks. Physical review letters 79 (20), 4038, publisher: APS.

Berkowitz, B., Scher, H., 1998. Theory of anomalous chemical transport in random fracture networks. Physical Review E 57 (5), 5858, publisher: APS.

Bour, O., 2002. A statistical scaling model for fracture network geometry, with validation on a multiscale mapping of a joint network (Hornelen Basin, Norway). Journal of Geophysical Research 107 (B6), 2113.

Bour, O., Davy, P., 1997. Connectivity of random fault networks following a power law fault length distribution. Water Resources Research 33 (7), 1567–1583.

Cherblanc, F., Ahmadi, A., Quintard, M., 2007. Two-domain description of solute transport in heterogeneous

porous media: Comparison between theoretical predictions and numerical experiments. Advances in Water Resources 30 (5), 1127–1143.

Cortis, A., Berkowitz, B., 2004. Anomalous transport in classical soil and sand columns. Soil Science Society of America Journal 68 (5), 1539–1548.

Davit, Y., Quintard, M., Debenest, G., 2010. Equivalence between volume averaging and moments matching techniques for mass transport models in porous media. International Journal of Heat and Mass Transfer 53 (21-22), 4985–4993.

de Dreuzy, J.-R., Davy, P., Bour, O., 2001. Hydraulic properties of two-dimensional random fracture networks following a power law length distribution: 1. Effective connectivity. Water Resources Research 37 (8), 2065–2078.

Demirel, S., Irving, J., Roubinet, D., 12 2019. Comparison of REV size and tensor characteristics for the electrical and hydraulic conductivities in fractured rock. Geophysical Journal International 216 (3), 1953–1973.

Ding, D., Benson, D. A., Paster, A., Bolster, D., 2013. Modeling bimolecular reactions and transport in porous media via particle tracking. Advances in Water Resources 53, 56–65.

Dorn, C., Linde, N., Le Borgne, T., Bour, O., Klepikova, M., 2012. Inferring transport characteristics in a fractured rock aquifer by combining single-hole ground-penetrating radar reflection monitoring and tracer test data. Water Resources Research 48 (11).

Gattinoni, P., Scesi, L., 2018. Short review of some methods for groundwater flow assessment in fractured rock masses. Acque Sotterranee-Italian Journal of Groundwater 7 (3), 7–17.

Geiger, S., Emmanuel, S., 2010. Non-Fourier thermal transport in fractured geological media. Water Resources Research 46 (7), publisher: Wiley Online Library.

Gouze, P., Puyguiraud, A., Roubinet, D., Dentz, M., 2020. Characterization and upscaling of hydrodynamic transport in heterogeneous dual porosity media. Advances in Water Resources 146, 103781.

Gouze, P., Puyguiraud, A., Roubinet, D., Dentz, M., 2023. Pore-scale transport in rocks of different complexity modeled by random walk methods. Transport in Porous Media 146, 139–158.

Jiang, C., Wang, X., Sun, Z., Lei, Q., 2019. The Role of In Situ Stress in Organizing Flow Pathways in Natural Fracture Networks at the Percolation Threshold. Geofluids 2019, 3138972.

Kang, P. K., Brown, S., Juanes, R., 2016. Emergence of anomalous transport in stressed rough fractures. Earth and Planetary Science Letters 454, 46–54, publisher: Elsevier.

Kang, P. K., Dentz, M., Le Borgne, T., Juanes, R., 2011. Spatial Markov model of anomalous transport

through random lattice networks. Physical review letters 107 (18), 180602, publisher: APS.

Kang, P. K., Dentz, M., Le Borgne, T., Juanes, R., 2015a. Anomalous transport on regular fracture networks: Impact of conductivity heterogeneity and mixing at fracture intersections. Physical Review E 92 (2), 022148, publisher: APS.

Kang, P. K., Dentz, M., Le Borgne, T., Lee, S., Juanes, R., 2017. Anomalous transport in disordered fracture networks: Spatial Markov model for dispersion with variable injection modes. Advances in Water Resources 106, 80–94, publisher: Elsevier.

Kang, P. K., Le Borgne, T., Dentz, M., Bour, O., Juanes, R., 2015b. Impact of velocity correlation and distribution on transport in fractured media: Field evidence and theoretical model. Water Resources Research 51 (2), 940–959, publisher: Wiley Online Library.

Kang, P. K., Lei, Q., Dentz, M., Juanes, R., 2019. Stress-induced anomalous transport in natural fracture networks. Water Resources Research 55 (5), 4163–4185, publisher: Wiley Online Library.

Lei, Q., Gao, K., 2018. Correlation between fracture network properties and stress variability in geological media. Geophysical Research Letters 45 (9), 3994–4006, publisher: Wiley Online Library.

Lei, Q., Gao, K., 2019. A numerical study of stress variability in heterogeneous fractured rocks. International Journal of Rock Mechanics and Mining Sciences 113, 121–133, publisher: Elsevier.

Lei, Q., Latham, J.-P., Tsang, C.-F., 2017a. The use of discrete fracture networks for modelling coupled geomechanical and hydrological behaviour of fractured rocks. Computers and Geotechnics 85, 151–176, publisher: Elsevier.

Lei, Q., Wang, X., 2016. Tectonic interpretation of the connectivity of a multiscale fracture system in limestone. Geophysical Research Letters 43 (4), 1551–1558, publisher: Wiley Online Library.

Lei, Q., Wang, X., Xiang, J., Latham, J.-P., 2017b. Polyaxial stress-dependent permeability of a three-dimensional fractured rock layer. Hydrogeology journal 25 (8), 2251–2262, publisher: Springer.

Liu, C., Zhang, L., Li, Y., Liu, F., Martyushev, D. A., Yang, Y., 2022. Effects of microfractures on permeability in carbonate rocks based on digital core technology. Advances in Geo-Energy Research 6 (1), 86–90.

Liu, R., Li, B., Jiang, Y., Yu, L., 2018. A numerical approach for assessing effects of shear on equivalent permeability and nonlinear flow characteristics of 2-D fracture networks. Advances in Water Resources 111, 289–300, publisher: Elsevier.

Majdalani, S., Chazarin, J.-P., Delenne, C., Guinot, V., 2015. Solute transport in periodical heterogeneous porous media: Importance of observation scale and experimental sampling. Journal of Hydrology 520,

52–60.

Min, K.-B., Rutqvist, J., Tsang, C.-F., Jing, L., 2004. Stress-dependent permeability of fractured rock masses: a numerical study. International Journal of Rock Mechanics and Mining Sciences 41 (7), 1191–1210, publisher: Elsevier.

Neuman, S., 2005. Trends, prospects and challenges in quantifying flow and transport through fractured rocks. Hydrogeology Journal 13 (1), 124–147.

Nick, H. M., Paluszny, A., Blunt, M. J., Matthai, S., 2011. Role of geomechanically grown fractures on dispersive transport in heterogeneous geological formations. Physical Review E 84 (5), 056301, publisher: APS.

Noetinger, B., Roubinet, D., Russian, A., Le Borgne, T., Delay, F., Dentz, M., de Dreuzy, J.-R., Gouze, P., 2016. Random walk methods for modeling hydrodynamic transport in porous and fractured media from pore to reservoir scale. Transport in Porous Media, 1–41.

Odling, N. E., 1997. Scaling and connectivity of joint systems in sandstones from western Norway. Journal of Structural Geology 19 (10), 1257–1271, publisher: Elsevier.

Odling, N. E., 2001. The scaling of hydraulic conductivity in rock fracture zones. Geophysical research letters 28 (15), 3019–3022, publisher: Wiley Online Library.

Painter, S., Cvetkovic, V., 2005. Upscaling discrete fracture network simulations: An alternative to continuum transport models. Water Resources Research 41 (2), publisher: Wiley Online Library.

Painter, S., Cvetkovic, V., Mancillas, J., Pensado, O., 2008. Time domain particle tracking methods for simulating transport with retention and first-order transformation. Water resources research 44 (1), publisher: Wiley Online Library.

Renshaw, C. E., 1997. Mechanical controls on the spatial density of opening-mode fracture networks. Geology 25 (10), 923–926, publisher: Geological Society of America.

Riva, M., Guadagnini, A., Fernandez-Garcia, D., Sanchez-Vila, X., Ptak, T., 2008. Relative importance of geostatistical and transport models in describing heavily tailed breakthrough curves at the lauswiesen site. Journal of contaminant hydrology 101 (1-4), 1–13.

Roubinet, D., de Dreuzy, J.-R., Davy, P., 2010. Connectivity-consistent mapping method for 2-D discrete fracture networks. Water Resources Research 46, W07532.

Roubinet, D., Demirel, S., Voytek, E. B., Wang, X., Irving, J., 2020. Hybrid analytical and numerical approach for modeling fluid flow in simplified three-dimensional fracture networks. Geofluids, 3583817.

Roubinet, D., Gouze, P., Puyguiraud, A., Dentz, M., 2022. Multi-scale random walk models for reactive

transport processes in fracture-matrix systems. Advances in Water Resources 164, 104183.

Rutqvist, J., Leung, C., Hoch, A., Wang, Y., Wang, Z., 2013. Linked multicontinuum and crack tensor approach for modeling of coupled geomechanics, fluid flow and transport in fractured rock. Journal of Rock Mechanics and Geotechnical Engineering 5 (1), 18–31, publisher: Elsevier.

Schiavo, M., 2023. The role of different sources of uncertainty on the stochastic quantification of subsurface discharges in heterogeneous aquifers. Journal of Hydrology 617, 128930.

Schiavo, M., Riva, M., Guadagnini, L., Zehe, E., Guadagnini, A., 2022. Probabilistic identification of preferential groundwater networks. Journal of Hydrology 610, 127906.

Smith, L., Schwartz, F. W., 1984. An analysis of the influence of fracture geometry on mass transport in fractured media. Water Resources Research 20 (9), 1241–1252, publisher: Wiley Online Library.

Sun, Z., Jiang, C., Wang, X., Lei, Q., Jourde, H., 2020. Joint influence of in-situ stress and fracture network geometry on heat transfer in fractured geothermal reservoirs. International Journal of Heat and Mass Transfer 149, 119216.

Sweeney, M. R., Hyman, J. D., 2020. Stress effects on flow and transport in three-dimensional fracture networks. Journal of Geophysical Research: Solid Earth 125 (8), e2020JB019754, publisher: Wiley Online Library.

Tran, E., Zavrin, M., Kersting, A. B., Klein-BenDavid, O., Teutsch, N., Weisbrod, N., 2021. Colloid-facilitated transport of 238pu, 233u and 137cs through fractured chalk: laboratory experiments, modelling, and implications for nuclear waste disposal. Science of The Total Environment 757, 143818.

Wang, C., Wang, X., Majdalani, S., Guinot, V., Jourde, H., 2020. Influence of dual conduit structure on solute transport in karst tracer tests: An experimental laboratory study. Journal of Hydrology 590, 125255.

Wang, Z., Li, H., Liu, S., Xu, J., Liu, J., Wang, X., 2023. Risk evaluation of co2 leakage through fracture zone in geological storage reservoir. Fuel 342, 127896.

Witherspoon, P. A., Wang, J. S., Iwai, K., Gale, J. E., 1980. Validity of cubic law for fluid flow in a deformable rock fracture. Water resources research 16 (6), 1016–1024, publisher: Wiley Online Library.

Yoo, H., Park, S., Xie, L., Kim, K.-I., Min, K.-B., Rutqvist, J., Rinaldi, A. P., 2021. Hydro-mechanical modeling of the first and second hydraulic stimulations in a fractured geothermal reservoir in pohang, south korea. Geothermics 89, 101982.

Zhao, Z., Jing, L., Neretnieks, I., Moreno, L., 2011. Numerical modeling of stress effects on solute transport in fractured rocks. Computers and Geotechnics 38 (2), 113–126, publisher: Elsevier.

589 Zhao, Z., Rutqvist, J., Leung, C., Hokr, M., Liu, Q., Neretnieks, I., Hoch, A., Havlek, J., Wang, Y., Wang,
590 Z., Wu, Y., Zimmerman, R., Apr. 2013. Impact of stress on solute transport in a fracture network: A
591 comparison study. Journal of Rock Mechanics and Geotechnical Engineering 5 (2), 110–123.
592 Zhou, Z., Roubinet, D., Tartakovsky, D. M., 2021. Thermal experiments for fractured rock characterization:
593 Theoretical analysis and inverse modeling. Water Resources Research 57 (12), e2021WR030608.